STUDIES OF SOLAR ATMOSPHERE

A thesis submitted to the
Punjabi University, Patiala
for the degree of
DOCTOR OF PHILOSOPHY
in the Faculty of Science

by

JAGDEV SINGH

Department of Astronomy and Space Sciences
Punjabi University, Patiala

1984

To M.K. Vainu Bappu

PREFACE

The invention of the solar coronagraph notwithstanding, a total solar eclipse remains the best means of studying the solar corona, especially the outer corona. The most distinctive feature of the solar corona is its high temperature, of the order of a few million degrees, and many properties of the corona can be explained in terms of this single fact.

Ever since 1869 when the coronal spectra were first seen, a spectroscopic study of the corona has been made at successive eclipses.

The profiles of coronal forbidden emission lines provide a large body of information about the physical characteristics of the solar corona. Green and red lines, 5303 Å [Fe XIV] and 6374 Å [Fe X], are the brightest visible coronal lines and have provided the bulk of information on the corona.

In spite of the fact that a large body of data is available from a number of eclipses, the data lack simultaneous high spatial and spectral resolution. Consequently, temperature structure and its variation with radial distance, mode of excitation of ions, and velocity pattern are but poorly understood. It is,

therefore, not possible to discriminate among existing theories concerning heating and energy balance of the solar atmosphere as well as energy sources required to drive the solar wind. Moreover, since the corona itself is a function of solar activity, a study of solar corona at different phases of solar activity can provide useful insight into coronal heating mechanisms and velocity flows.

With a view to obtaining insight into physical processes in the corona, we observed solar corona in red and green lines at two total solar eclipses, the Indian eclipse of 1980 when the solar activity was maximum and the Indonesian eclipse of 1983 when the solar activity was low. Multislit, high dispersion, high spatial resolution spectroscopy was used to obtain the red line profiles at the 1980 eclipse and the red and green line profiles at the 1983 eclipse. The results from these two eclipses are discussed in this work.

My first thoughts go to the late Dr M.K. Vainu Bappu, who introduced me to the subject, who suggested that I work on the solar eclipses, who guided me at every stage, but did not live to see the completion of this work. I thank Mrs Yemuna Bappu for her kindness and best wishes.

After Dr Bappu's death on August 19, 1982, Dr K.R. Sivaraman supervised the work and helped in the selection of the experiments. He took keen interest in the completion of the work and checked the final manuscript in great detail. Professor J.C. Bhattacharyya gave many useful tips. My old teacher Professor H.S. Gurm was ready with suggestions whenever I needed them.

Dr T.P. Prabhu was of great help at the 1980 eclipse site and in reduction of data. Mr P.S.M. Aleem assisted with the testing of the instruments and Dr A.K. Saxena with the observations at the 1980 eclipse. Drs K.R. Sivaraman and R. Rajamohan and Mr F. Gabriel helped with the 1983 observations. Mr A.V. Raveendran provided computer programmes for data reduction. I have had many useful discussions with Mr P. Venkatakrishnan and Dr P.K. Raju. Dr R.K. Kochhar was a constant source of encouragement and went through an earlier draft.

The success of the experiments owed much to the fabrication skills of Messrs A. Charles, F. Gabriel, A. Arockiam, T. Johnson and A.J. Soosairaj. Mr K.S. Ramamoorthy assembled the power supply for driving the stepper motor. Miss K. Padmavathi and

Mrs Meena Krishnan typed the rough draft; the final typing is Mr. A. Mohammed Batcha's handiwork. Mr S. Muthukrishnan drew the figures. Ms A. Vagiswari, Mr H.N. Manjunath, Mrs and Mr R. Krishnamoorthy, and Messrs A. Elangovan, S. John and P.N. Prabhakar helped with the production of the thesis.

(Jagdev Singh)

CONTENTS

CONTENTS

--

CHAPTER 1

INTRODUCTION

1.1. Historical background

The sun is not merely one among the several billion stars in our Galaxy. To the human-kind the sun is something unique; apart from being the source of life on the earth, it is the closest star. It is close enough for its surface features to be studied in fine detail and its space environment probed. Its radiations are sufficiently intense to permit a minute examination of its spectrum. And thanks to the fortunate circumstances of total solar eclipses,the sun's atmosphere can also be studied in detail. During the total solar eclipse the lunar shadow on the earth darkens the sky to such an extent that the corona appears as a large brilliant halo surrounding the eclipsed sun. In total brightness the corona is comparable to the full moon.

According to a Babylonian account, probably of the eclipse of July 31, 1063 BC, "... the day was turned into night and there was fire in the midst of heaven ...". Plutarch wrote abqut the eclipse of December 27, 83 AD: "There always appears around the circumference

of the moon some light that does not permit total darkness". Kepler in 1608, Cassini in 1706 and Halley in 1715 commented on the existence of the corona, but Halley could not decide whether it was connected with the sun or the moon (see Mitchell 1935).

At the 1842 eclipse Francis Baily an enthusiastic amateur astronomer, who had already become well known among the eclipse observers through Baily's beads, described in glowing terms the solar corona and the protuberances thus: "I was ... electrified at the sight of one of the most brilliant and splendid phenomena that can be imagined. For at that instant the dark body of the moon was suddenly surrounded with a corona, or kind of bright glory". Since then the corona has been the subject of serious scientific study.

The total solar eclipse of July 18, 1860 is a landmark in the progress in the studies of the solar atmosphere. At this eclipse, the chromosphere, the corona and the prominences were successfully photographed for the first time. The Italian astronomer Father Angelo Secchi and the British amateur astronomer Walter de la Rue photographed the eclipsed sun from two sites in Spain some 400 km apart. De la Rue used

the heliograph from Kew enlarging the image before it reached the photographic plate, while Secchi employed a six-inch refractor without enlargement. By comparing their photographs they concluded that the corona and the prominences were real physical structures belonging to the sun and not an optical illusion produced by the earth's atmosphere. Secchi from an examination of his own and of de la Rue's photographs noticed the existence of a layer of material surrounding the sun from which arose the red flares. This layer was later, in 1869, named chromosphere by the English Astronomer Royal Joseph Norman Lockyer. It was at this eclipse that the corona was first viewed in polarized light, by Secchi and Prazmowski. The success of the 1860 eclipse coincided with the birth of the new science of spectroscopy, which was to play an increasingly significant role in the solar studies which in turn stimulated laboratory experiments. In 1859 the German physicist Gustav Kirchoff provided an explanation for the solar absorption spectrum which Joseph Fraunhofer at Munich had obtained in 1817.

It was at the eclipse of August 18, 1868 that the spectroscopic methods were applied to eclipse observations for the first time. The most successful efforts were those of the French astronomer Pierre Jules Janssen,

who observed this eclipse from India. The slit of Janssen's spectroscope directed to the edge of the sun revealed the spectrum of the prominences consisting of a series of bright emission lines. The most prominent among these were the three lines - the red and the blue lines belonging to hydrogen, and an equally brilliant yellow line. This yellow line could not be identified with any of the elements known to exist at that time. It was ascribed by Norman Lockyer as due to helium, named after helios, the sun.

At the North American eclipse of August 7, 1869 Charles Young and Harkness independently discovered an emission line in the green in the coronal spectrum besides the known continuous spectrum. Young identified the green line with the line numbered 1474on Kirchhoff's scale. A few years later, Young identified this green line with the violet component of the line 1474 on the Kirchhoff's scale, the red component being known to be due to iron. This was still a misidentification but solved the contemporary problem that it was not necessary to assume the iron vapour to extend as much as hydrogen in the solar atmosphere. The green line was, therefore, ascribed to coronium, a new element.

According to Kirchhoff's law, the absorption lines arise in a 'reversing layer' in the solar atmosphere. If this reversing layer is seen without the hot continuum background emission of the solar photosphere, the Fraunhofer lines would be seen in emission. During the beginning and the end of a total solar eclipse, as the moon covers most of the sun except for a thin crescent of the reversing layer, this phenomenon of the reversal of the Fraunhofer spectrum should be observable. This reversal-bright lines on a dark background - was seen by Young of Princeton at the eclipse of December 22, 1870. Since the emission spectrum is visible only for a few seconds, Young called it a 'flash spectrum'. In 1871, for the first time, and due to a suggestion by Young, a slitless spectroscope was tried. With the help of such an instrument at mid-totality, the emission lines appeared as rings of light, from the extent of which one could ascertain the height of the various gases forming the corona. With the help of photography, Lockyer showed in 1871 that hydrogen extended uniformly about the sun to the enormous height of 20000 miles, and the green coronal line arose at a still larger height of 30000 miles.

The eclipse of July 29, 1878 brought home the fact that the corona was not constant in brightness

and shape. The 1878 corona was about a factor of 10 less luminous than the corona of 1870 or 1871. The decrease in brightness was accompanied by significant changes in shape. In 1871 the corona was nearly circular. In 1878, the streamers along the sun's axis were much shorter. Along the sun's equator on one side the streamers extended to more than ten million kilometres. Subsequent eclipses established that the overall shape of the corona changed systematically in phase with the 11-year sunspot cycle. At the eclipse of May 6, 1883 in India, Janssen showed that the coronal light has the same absorption spectrum as the photosphere. It was at this eclipse that the flash spectrum was also first successfully photographed, but only a few of the brighter lines were recorded. Whereas the first coronal spectra had been viewed as early as 1869, it was not still 1893 that they were photographed. At the eclipse of 1898 in India, Naegamvala stationed at Jeur obtained very good high resolution photographs of solar corona, and chromospheric and coronal spectra. Fowler's spectrum of the corona obtained during the eclipse showed well the 1474 line. Examining the spectrum Lockyer showed that the wave-length of 1474 line had been wrongly measured earlier and was not connected with the Fraunhofer line. By 1898 more than ten coronal lines had been discovered.

There was also the strong suspicion that all these lines did not originate from the same hypothetical element, coronium.

The year 1930 marks a turning point in coronal studies. In that year French astronomer Bernard Lyot succeeded in constructing a working coronagraph. Lyot's achievement had behind it more than 50 years of efforts by many workers to observe the corona outside of an eclipse. The basic difficulty in the observation of the solar corona without an eclipse is due to the presence of an intense spurious scatter halo around the sun, produced by light from the solar disc scattered in the terrestrial atmosphere and in the observing telescope itself. Lyot solved the problem by minimizing the brightness of the scatter halo by optical refinements in the observing telescope and choice of an observing site with a very clear sky. Later, Lyot (1950) devised a sensitive photoelectric instrument capable of detecting and measuring the coronal green line through the scattered light of an ordinary telescope and a smoky sky. In 1932, Lyot made an observation that led to the revolutionary concept of the corona being much hotter than the photosphere. Using a spectrograph with a dispersion higher than could be used during an eclipse, he measured the profile of

the green coronal line and reported that its width was 0.8 Å and it was very regular. A few years later he suggested that the broadening was thermal. He was unable to compute the temperature from the line profile, however, because he did not know the atomic weight of the line-emitting ion (Lyot 1939).

Grotrian (1931) noted that in the spectrum of inner corona the H and K absorption lines of Ca^+ were replaced by shallow depression in the continuum extending from below 3900 Å to above 4100 Å. He pointed out that the broadening would indicate a velocity in the coronal electrons of 7.5×10^3 km s^{-1}, compared to the average thermal velocity for electrons at 6000 K, of 5.5×10^2 km s^{-1}. The high electron velocities may be thermal or due to motions along lines of force. He did not pursue the idea of high temperature corona.

Clues to solving the mystery of coronal lines came from unexpected quarters. Bowen in 1935 identified some of the lines from nova Pictoris 1925 as forbidden lines of Fe VI. In 1939, Bowen and Edlen identified the remainder of the nova lines as due to forbidden transitions in Fe VII. In the mean time, Adams and Joy discovered beyond doubt five coronal lines in the spectrum of the recurrent nova R S Ophiuchi during its 1933 brightening. These two discoveries suggested to

Grotrian that the coronal lines might perhaps also be emitted in forbidden transitions of highly ionized elements. Edlen had already studied the spectra of some ions and identified some lines and terms in Fe X. Following Edlen's results, Grotrian identified red line as due to Fe X ion and noted that its behaviour was different from that of most coronal lines, with the exception of the line at 7892 Å that had been recently discovered by Lyot. Edlen had also determined energy levels for Fe XI. The line at 7892 Å was interpreted as due to Fe XI by Grotrian. Following Grotrian's lead Edlen (1942) identified 19 out of 23 known coronal lines, all as forbidden transitions in highly ionized atoms of familiar elements, principally iron, nickel and calcium. These emission lines are important only when the medium is extremely tenuous.

The width of the coronal line profile measured by Lyot, together with the identification of the emitting ions by Grotrian and Edlen, provided evidence for placing the temperature of the corona at one million degrees or more. By 1945 the concept of a hot plasma had found general acceptance (see Table 1 for summary of landmarks in coronal studies). From observations of many eclipses and with coronograph it became evident that the coronal spectrum has three components: an

emission line spectrum radiated by hot ions (the E-corona), a polarized continuum as a result of Thompson scattering of free coronal electrons (the K-corona) and a Fraunhofer spectrum scattered from cool interplanetary dust particles (the F-corona).

1.2. The present status of the knowledge of solar corona

The two outstanding problems concerning the corona are (i) the precise measurement of its high temperature and (ii) the identification of coronal heating mechanisms. We shall be concerned here only with the problem of measuring the coronal temperature. A number of methods are available to measure the temperature and are discussed below. Emission line profiles, which are the subject of this study, are discussed in some detail in Section 1.3.

The temperature of the solar corona

The most distinctive feature of the solar corona probably is its high temperature and many of the properties of the corona can be explained in terms of this single fact. The temperature as applied to the corona had a broader connotation based on the techniques employed and can be estimated in the following ways:

i) The average temperature

ii) The ionization temperature

iii) The radio temperature

iv) Temperature from spectral intensity of the K-corona

v) Temperature from ultraviolet observations

vi) The line-width temperature

i) The average temperature: Even though the corona is known to be highly structured, one can still meaningfully talk of an 'average' corona. It is normally assumed that the average corona is spherically symmetric. In other words, the average brightness can be interpreted in terms of an average electron density in an assumed spherically symmetric distribution. Since hydrogen and helium in the corona are known to be nearly fully ionized, the electron density is directly proportional to the total density. Electron density distribution can be obtained from an analysis of the continuum of the K-corona. Then if the corona is in hydrostatic equilibrium, the pressure gradient balances the acceleration due to gravity at any point.

$$\frac{dp}{dr} = - \mu \, m_H \, n_e \, g_\odot \, (R_\odot/r)^2 \, . \qquad .. \ (1.1)$$

Here $R_\odot$ is the solar radius; $g_\odot$, the acceleration due to gravity; μ, the mean molecular weight; m_H, the mass of the hydrogen atom; and n_e, the average electron density. For an isothermal corona obeying perfect gas law, we have (Athay 1975)

$$T = \frac{\mu\, m_H\, g_\odot\, R_\odot}{k} \left[\frac{d \log n_e}{d\,(R_\odot/r)}\right]^{-1} \qquad .. (1.2)$$

where k is the Boltzmann constant.

According to equation (1.2), in a plot of log n_e vs $(R_\odot/r)$, a constant temperature is represented by a straight line. In the empirical model of van de Hulst (1953) the sunspot minimum polar corona seems well represented by a temperature of 1.0×10^6 K. For the sunspot maximum corona, $r/R_\odot \leq 2.5$ corresponds to $T = 1.4 \times 10^6$ K and $r/R_\odot > 2.5$ to $T = 0.97 \times 10^6$ K. Although factors like the magnetic pressure, departure from spherical symmetry, the unlikelyhood of the corona remaining isothermal over large distances and the expansion of the corona would make the corona at any point in time depart from the simple spherically symmetric, hydrostatic model, the mean corona at a given solar latitude does appear to be broadly consistent with the model, atleast out to about 2.5 $R_\odot$ from the solar surface.

ii) The ionization temperature: The most important consequence of the high temperature of the corona is its state of high ionization. One can postulate a steady state relation between the degree of ionization and temperature for each of the various heavy ions in the corona. One can set the rate at which atoms change from a lower to the next higher degree of ionization equal to the rate at which they return from that state.

If n_i is the number density of ions of a given element in the ith state of ionization, n_{i+1} the number density in the next stage of ionization, then in the steady state,

$$\frac{n_{i+1}}{n_i} = \frac{I}{R} \qquad .. (1.3)$$

where I and R are rate factors for ionization and recombination, respectively, and are both functions of temperature. If I(T) and R(T) are known, an observational determination of the relative number of ions in two successive states of an element provides an evaluation of the electron temperature. To deduce the relative ion concentration from observational data, one must be certain that the spectral lines observed for different ions originate from the same geometrical

regions. This unfortunately is not possible. Indeed, there is every reason to suppose that different ions will be distributed differently in space because of the temperature gradients. The two coronal lines most frequently used for coronal studies are the green line at 5303 Å of Fe XIV and the red line at 6374 Å of Fe X. There are enough indications that [Fe X] and [Fe XIV] emissions do in fact arise in volume elements that are systematically different (Athay 1975). A precise evaluation of I and R requires a knowledge of the atomic parameters. In earlier attempts, it was assumed that recombination is purely radiative. This gave lower temperatures for the corona than were determined from most other methods of observation. This difficulty was resolved when Burgess (1964) pointed out the role of dielectronic recombinations whereby a free electron becomes bound without emitting any radiation by free-bound transitions. When allowance is made for dielectronic recombinations, each ion achieves its maximum population at approximately twice the temperature that was found when radiative recombinations alone are considered (Burgess and Seaton 1964). Goldberg, Dupree and Allen (1965) suggested incorporation of auto-ionization into the ionization equilibrium models. Jordan's (1969) ionization equilibrium

computations which are the most recent ones give the maximum concentration of Fe XIV and Fe X at temperatures of 2.3×10^6 K and 1.3×10^6 K, respectively. Under the assumption that Fe XIV is commonly the most abundant ion which is consistent with the mean intensity of the 5303 Å line relative to other coronal lines, the most common ionization temperature of the corona turns out to be 2.3×10^6 K. At the same time, however, it must be recognized that ionization temperatures close to 1.3×10^6 K (Fe X) are also relatively common in the normal corona.

iii) <u>The radio temperature:</u> The most direct method of determining the coronal temperature is the measurement of the radio brightness temperature. It is also one of the most accurate methods.

From the flux density at a given wavelength and the dimensions of the solar corona, radio brightness temperature T_b can be computed. If the corona is assumed to be isothermal, with an optical depth τ, then the coronal temperature is given by

$$T_b = T\,(1-e^{-\tau}) \quad . \qquad \ldots (1.4)$$

It is only for wavelength in the range 1-5 m that τ exceeds unity and $T_b \approx T$. At shorter wavelengths the corona is transparent and is observed against the

chromosphere and transition region radiation. At longer wavelengths the complex index of refraction bends the rays away from the higher density regions of the low corona, and the corona becomes transparent again. Thus, outside the wavelength range 1-5 m, the brightness temperature is less than the true coronal temperature.

Radio measurements of central disc temperatures cannot provide a good angular resolution. The sun is an irregular radio source so that the brightness distribution over the disc may differ significantly from the average distribution. Therefore, it is not possible to infer the central disc brightness from the integrated brightness.

Leblanc and LeSqueren (1969), from observations at 178 cm, obtained coronal temperatures of 1.1×10^6 K at sunspot minimum and 1.8×10^6 K for the 'quiet' corona at sunspot maximum.

iv) Temperature from spectral intensity of the K-corona: Cram (1976) suggested a method to determine the electron temperatures from spectral intensities of the K-corona. K-coronal spectrum is formed as the photospheric light is scattered by energetic coronal electrons. The Doppler shifts suffered by these

scattered photons broaden the absorption lines in the original Fraunhofer spectrum and produce the K-coronal spectrum. Cram's calculated spectra for a spherically symmetric isothermal corona at four electron temperatures brings out two interesting features. First, there exist spectral nodes, that is, wavelengths at which the intensity is independent of the assumed electron temperature. Second, the spectra undulate about these nodes with an amplitude that is related to the electron temperature. Thus, the ratio of two measured intensities, one at a nodal wavelength and the other at a near-by wavelength, can uniquely determine the electron temperature. The intensity measurements require a very great accuracy because an error of ± 0.2 per cent in the intensity ratio translates into an uncertainty of $\pm 0.1 \times 10^6$ K in the coronal electron temperature. In standard photometric techniques, an error of 5 per cent is quite common as shown by Menzel and Pasachoff (1968) while searching for residual depressions from H and K lines of Ca^+. To achieve the required sensitivity, Keller (1982) used an instrument with an array of silicon photo diodes during the Indian eclipse of 1980 and tried to measure the K-coronal spectral intensity but without success.

v) Temperature from ultraviolet observations:

Observations made by rocket and satellite experiments have provided information at ultraviolet and extreme ultraviolet wavelengths. Since some of the ionic species give rise to certain combinations of lines in the EUV region which are sensitive to temperature, the intensity ratios of these lines provide direct information on the local values of temperature and density in the regions from where the emission arises, independent of the geometry of the emitting region. The interpretation of intensity ratios requires a knowledge of accurate atomic parameters. This type of analysis has a great advantage in the case of active events in which geometry is often unknown and for which only limited data may be available.

In lithium-like ions the 2p and 3p levels differ in excitation energy by a large factor. The excitation of such levels is primarily by electron collisions with ions in the ground state. The intensity of an optically thin EUV emission line observed above the limb (Withbroe 1970) is given by

$$I(x) = 1.73 \times 10^{-16} A f \int_{-\infty}^{\infty} G(T_c)\, N_e^2\, ds \quad , \ldots (1.5)$$

where x is the distance from the centre of the solar disc in units of solar radius; A is the abundance of

the element forming the line, measured relative to hydrogen; f is the oscillator strength; G(T) is a function that depends on the fraction of atoms in the ionization state producing the line, on the Gaunt factor, and on the excitation potential of the line; and $ds = rdr/\sqrt{r^2-(xR_\odot)^2}$.

Assuming that the coronal plasma along the line of sight is isothermal, we get

$$I(x) = 1.73 \times 10^{-16} Af\, G(T_c) \int_{-\infty}^{\infty} N_e^2\, ds \quad . \qquad .. (1.6)$$

The ratio of the intensities of two spectral line 1 and 2 observed at the same height above the limb is given by

$$\frac{I(x)_1}{I(x)_2} = \frac{A_1}{A_2} \frac{f\, G(T_c)_1}{f\, G(T_c)_2} \quad . \qquad .. (1.7)$$

If we substitute the values of the quantities A, f and the Gaunt factor used in evaluating G(T) we can estimate temperature from the measured line intensity ratio. The orbiting solar observatory and Skylab have provided data in the XUV and EUV regions. Withbroe (1975), from the measurements of XUV line intensities, has shown that mean coronal temperature ranges from (1.5 to 2.1) x 10^6 K. Reeves, Vernazza and Withbroe (1976) obtained a coronal temperature of 1.1 x 10^6 K

from the intensity ratio of Mg X and O VI lines. Harvard experiment on Skylab yielded the intensities of O VI and Mg X. Mariska and Withbroe (1978) found that the observed intensity ratio indicates a temperature of about 1.2×10^6 K by using photospheric abundances and EUV abundances give a temperature of 2.8×10^6 K. Thus a small uncertainty in the abundances reflects a large uncertainty in the deduced coronal temperature. Therefore, they concluded that Mg X/O VI will allow any coronal temperatures between 1×10^6 and 3×10^6 K at 1.05 $R_\odot$. They also showed that the ratio of Si XII/Mg X suggests a coronal temperature of about 2×10^6.

vi) Line-width temperatures: The temperature of the corona can also be measured by the use of line profiles. Consider a region in space small enough to be homogeneous yet large enough to contain a considerable number of each species of coronal particles. Let n_i be the number of particles of the ith kind with a line-of-sight velocity $v_{x,i}$. If $\bar{v}_{x,i}$ is the rate of drift of this species, either through wind or diffusion, then $V_{x,i} = v_{x,i} - \bar{v}_{x,i}$ may be considered to be the 'thermal' line-of-sight velocity of a particle in the species.

Equating the momentum transferred in unit time to the partial pressure exerted by the species, we get

$$T = \frac{m_i \bar{V}_{x,i}^2}{k} = \frac{m_i}{k} \frac{c^2(\Delta\lambda_1)^2}{\lambda^2} \qquad .. (1.8)$$

where m_i is the mass of the ion and $\Delta\lambda_1$ is measured from the mean position rather than the normal position of the centre of the profile. Equation(1.8) is applicable to any profile, Gaussian or not, and indicates that line-profile measurements will give temperatures that are consistent with the gas laws even though the gas may not be described by a Maxwell-Boltzmann distribution of velocities.

If the distribution is Boltzmannian and profiles Gaussian, the parameter $\Delta\lambda_D$, the Doppler half width, is related to the temperature by

$$T = \frac{m_i c^2}{2k} \frac{(\Delta\lambda_D)^2}{2} \qquad .. (1.9)$$

or

$$T = \frac{m_i c^2}{2k} \frac{\Delta\lambda^2}{\lambda^2 4 \ln 2} \quad , \qquad .. (1.10)$$

where $\Delta\lambda$ is the full width at half maximum.

The determination of coronal temperature by line-profile analysis has the advantage over degree-of-

ionization technique that the only atomic parameter involved is the atomic weight of the emitting ion. Furthermore, since the corona is optically thin in the visual emission lines, the profile breadths may be interpreted unambiguously as arising from motion of the emitting ions. But the line broadening may not be entirely due to thermal motions; a part of the line broadening could be nonthermal in origin. If V_t is the magnitude of the nonthermal, random velocity, then the true broadening temperature is given by

$$\frac{2\,kT}{m_i} + V_t^2 = \frac{c^2\,\Delta\lambda^2}{\lambda^2\,4\,\ln 2} \quad . \qquad .. \ (1.11)$$

For the [Fe XIV] line typical values for the thermal and apparent broadening temperatures are 1.8×10^6 K and 2.5×10^6 K respectively (Athay 1975). This gives for the random velocity a value $V_t = 16$ kms^{-1}. By comparison, the mean thermal velocity for T = 1.8×10^6 K is 23 kms^{-1}.

1.3. Profiles of coronal emission lines

The profiles of coronal forbidden emission line can provide a large body of information about the physical characteristics of the solar corona. These line profiles can be used to determine the spatial dependence of the kinetic temperature, and contribution

of turbulent velocities towards line broadening, as already seen (Section 1.2). Coronal emission lines in the visual spectrum have been extensively studied during eclipses and using the coronagraph outside of eclipse since its invention by Bernard Lyot in 1930. The green and the red coronal lines, 5303 Å and 6374 Å, are the brightest visible lines and have provided the bulk of information on the corona. Observations made with coronagraphs outside an eclipse suffer from superposed skylight and instrumentally scattered light, both of which contain the Fraunhofer spectrum. Thus the green line observed with a coronagraph is blended with a Fraunhofer line and the profile must be suitably corrected for this blend. Observations made at an eclipse, however, are free from this defect and are thus very useful in complementing the coronagraph observations. Moreover, scattering of residual stray light within the coronagraph masks all but the brightest inner portions of the corona, leaving the study of the fainter, outer corona exclusively to eclipse observations. Indeed, during a total solar eclipse the scattered light intensity near the sun is reduced by about three orders of magnitude which makes possible observations of the emission corona to more than 2 $R_\odot$.

Line profile studies from eclipse observations have almost exclusively been carried out with Fabry-Perot interferometer both in two dimensional mode by photographic technique and at few specific locations by photoelectric scan methods. About 20 unsuccessful attempts of interferometric observations are on record including those of Wright and Heber D. Curtis who tried specially coated Fabry-Perot etalons at the eclipses of 1923, 1925, 1926 and 1929 (Mitchell 1935). Kaliniak (1949) used a slit spectrograph in conjunction with a Fabry-Perot interferometer but could not resolve the green line. The first successful interferometric measurements of the coronal lines were by Jarrett and von Klüber at the June 30, 1954 eclipse. They used the classical multi-fringe Fabry-Perot interferometer with photographic recording in which the etalon behaves as an angular filter. Microdensitometry of the fringes yielded line profiles in several regions of the corona. Their 5303 Å interferograms seem to indicate a decrease in the line widths with increasing distance from the sun (Jarrett and von Klüber 1955). These line widths yield values ranging from 2.2×10^6 to 5×10^6 K for kinetic temperature, with most values around 2.5×10^6 K, for regions between 1.05 and 1.3 solar radii from the solar centre. Again, at the solar maximum eclipse of

October 12, 1958 they observed the corona both in the red and green coronal lines (Jarrett and von Klüber 1961). The mean temperature from the green line was about 3.2×10^6 K and from the red line 3.5×10^6 K. They did not find any evidence of change in line widths with distance from the limb. Subsequently Delone and Makarova (1969, 1975), Hirschberg, Wouters and Hazelton (1971), Marshall and Henderson (1973), Liebenberg, Bessey and Watson (1975), Kim and Nikolsky (1975), Desai, Chandrasekhar, and Angreji (1982), Smartt, Zirker and Mauter (1982) used a Fabry-Perot etalon for line profile studies during various solar eclipses. The interferometric results are summarized in Table 2. The measurement of line profiles, observed at these seven eclipses, give different values of line widths implying different temperatures varying between (2.5 and 4.5) $\times 10^6$ K. Only Delone and Makarova (1965, 1969) and Desai, Chandrasekhar and Angreji (1982) have reported large scale macroscopic mass motions in the solar corona with a velocity of about 70 - 100 kms^{-1}, whereas most of other observers do not find any large line-of-sight velocity. Turbulent velocity of the order of 25 kms^{-1} has been reported by many authors by expressing the excess line width in terms of turbulence. This seems to be real, but the existence of the turbulence must be established independently. Jarrett and

von Klüber (1955) find decrease in line width with increasing distance where as Kim and Nikolsky (1975) report a result opposite of this. Others have not been able to draw any definite conclusions from their observation regarding the relation of line width with distance. Therefore, observations with better spatial as well as spectral resolution are required to arrive at definite conclusions regarding the temperature structure of the solar corona.

The Fabry-Perot technique has the advantage of simultaneous registration of interference fringes over most of the corona, from which the line profile can be evaluated. But, it has the inherent disadvantage that the contribution of the Doppler-shifted elements to the line profile cannot be uniquely determined. This limitation is overcome by using a slit because the finite width of the slit permits the acquisition of information only along the coronal emission regions intercepted by its length. But this in turn means that the multiplicity of spatial information provided by the Fabry-Perot technique would be missing. Procedures to minimize this handicap, however, do exist and have been used for other purposes at the recent solar eclipses by Livingston, Harvey and Doe (1970). Coronal spectroscopy by multislit technique

has been used by the Kitt Peak investigators for measuring the coronal rotation. It is, however, a technique that can be utilized to provide a good two-dimensional coverage of the corona by judicious choice of instrumentation and spatial sequencing at the eclipse and has all the advantage to offer which the standard slit spectroscopy possesses over its slitless counterpart.

We have used the multislit technique to obtain the line profiles of selected coronal emission lines during the total eclipses of February 16, 1980 in India and of June 11, 1983 in Indonesia.

Chapter 2 describes the 1980 eclipse observations, where 6374 Å line profiles were obtained. Chapter 3 and 4 deal with the results obtained at the 1983 eclipse. The 5303 Å line profiles are discussed in Chapter 3, and coronal rotation derived from the 6374 Å line in Chapter 4. Concluding remarks are given in Chapter 5. In this Chapter we present a discussion of these results and the suggestions of observing programmes that need to be undertaken in future eclipses to provide answers to many questions about the physical nature of the corona.

Table 1

Landmarks in coronal studies

1842	Corona highlighted (Baily)
1860	Corona, chromosphere and prominences photographed (Secchi and de la Rue)
1860	Corona seen in polarized light (Secchi and Prazmowski)
1868	Prominence spectra (Janssen)
1869	Green coronal line discovered (Young and Harkness)
1870	Flash spectrum (Young)
1878	Coronal shape and intensity related to the solar cycle.
1883	Fraunhofer spectrum in corona (Janssen)
1883	Flash spectrum photographed
1893	Coronal spectrum photographed
1898	313 lines in flash spectrum photographed (Evershed)
1930	Coronagraph (Lyot)
1932	Line width of green line measured (Lyot)
1935	Forbidden lines identified in nova (Bowen)
1941	Coronal lines explained (Edlen)

Table 2

Interferometric observations of the solar corona

S. No.	Eclipse Date	Authors	Wave-length in Å	Line width temp. (in units of 10^6 K)	Remarks
1.	2.	3.	4.	5.	6.
1.	June 30, 1954	Jarrett and von Klüber (1955)	5303	2.2 - 5.0 (most frequent value = 2.5)	Decrease of line widths with increasing distance from the sun.
2.	Oct. 12, 1958	Jarrett and von Klüber (1961)	5303 6374	3.2 (mean) 3.5 (mean)	No evidence for change in line widths with distance.
3.	May 30, 1965	Delone and Makarova (1969)	5303 6374	6.8 - 16.0 0.3 - 11.9 (most frequent value = 3.9)	67% of 6374 Å - line profiles not Gaussian. Turbulent velocity $\backsim$ 26 kms^{-1}. Large scale mass motions, with V_t = 70 kms^{-1} in the active regions.
4.	May 30, 1965	Liebenberg, Bessey and Watson (1975)	5303 5694 6374	1.6 - 4.2	Air-borne experiment. Turbulent velocity $\backsim$ 25 kms^{-1}, turbulent velocity decreases with radial distance.

Table 2 - continued

1.	2.	3.	4.	5.	6.
5.	Sept..22, 1968	Delone and Makarova (1975)	5303	4.5 (most frequent value)	Interferograms obtained in polarized light. Large line-of-sight velocities $\backsim$100 kms^{-1} observed.
6.	March 7, 1970	Hirschberg, Wouters and Hazelton (1971)	5303	2.5 - 4.8	Doppler shifts indicate a vortex velocity of 6 kms^{-1}.
7.	March 7, 1970	Marshall and Henderson (1973)	5303 6374	3.7 (mean) 2.8 (mean)	Some suggestion of change in line width with time. No large scale macroscopic motions in the solar corona.
8.	July 10, 1972	Kim and Nikolsky (1975)	5303 5876 6374	3.2 - 4.8 2.7	D_3 emission only in chromosphere. Green line widths show an increase of non-thermal velocities with a gradient of 1-2 kms^{-1} per 0.1 $R_\odot$.
9.	Feb. 16, 1980	Desai, Chandrasekhar and Angreji (1982)	5303	1.1 - 4.7	Large scale macroscopic mass motion with velocity of (30-50) $\pm$ 7 kms^{-1}.
10.	Feb. 16, 1980	Smartt, Zirker and Mauter (1982)	5303	-	Experiment for velocity and intensity distribution associated with coronal loops.

CHAPTER 2

THE 1980 CORONA: 6374 Å LINE PROFILE

2.1. Introduction

For a detailed study of the line profiles in the solar corona, we chose the coronal emission line 6374 Å [Fe X], because of the advantage of its brightness which makes it possible to record the line far out in the corona. The characteristics of the red coronal line are (Allen 1973)

Transition	= $3p^5$, $^2P_{3/2} - {}^2P_{1/2}$
Transition probability	= 69 s^{-1}
Excitation potential	= 1.94 eV
Ionization potential	= 235 eV
Average equivalent width of eclipse coronal line in terms of electron scatter (K) continuum	= 5 Å
Temperature at which Fe X ion is most abundant (Jordon 1969)	= 1.3 x 10^6K

The experiment was set up a few hundred metres away from the central path of totality at Jawalagera (Long. 76° 52' 52"E; Lat. 15° 50' 57"N; elevation 346 metres) in a farm.

The eclipse parameters at the site were

	Local time			P	V	Solar Altitude	Solar Azimuth
First contact	14^h	21^m	14^s	244°	202°	53°	223°
Second contact	15^h	41^m	14^s	54°	354°	38°	240°
Third contact	15^h	44^m	03^s	256°	196°	37°	241°
Fourth contact	16^h	53^m	45^s	66°	358°	22°	249°

Duration of the totality = $2^m\ 49^s$

Magnitude of the eclipse = 1.038

Width of the eclipse path = 127 km

Local time = U.T + $5^h\ 30^m$

P = angle of contact on the solar disc measured from the north point through east.

V = angle measured from the vertex of the solar image. The sky was perfectly blue on the day of the eclipse.

2.2. Instruments

The experimental set up consisted of a coelostat with a single 45 cm mirror of Zerodur glass, feeding light on to a 14 cm aperture objective, a doublet corrected for 6500 Å and of 140 cm focal length. The R A circle was driven by friction through a metallic

tape which in turn was driven by a well regulated stepper motor. The tracking by the coelostat was good to the extent that the image remained practically stationary atleast for ten minutes. The objective, mounted on a platform capable of movement in two perpendicular directions in the horizontal plane, one for focussing the image and the other for shifting the geometrical position of the image relative to the spectrograph slits, formed a 13 mm image in the slit plane (Figure 1). The spectrograph with multislits used a 600 lines mm^{-1} grating and 100 cm focal length achromatic doublet and operated in the Littrow mode providing a dispersion of 2.5 Å mm^{-1} in the fourth order red region. Five entrance slits, each separated by 5 mm from its neighbour, gave a good coverage of the corona extending upto 1.5 $R_\odot$ in the direction normal to the length of the slit. The slit length of 34 mm provided the possibility of recording the spectra of solar corona upto 2.6 $R_\odot$ in the east-west direction. The orientation of the multislit was along position angle 89.5°, so that the longer dimension of the slits were parallel to the solar equator. An interference filter with 9.5 Å pass band and peaked transmission at 6377 Å was mounted in front of the multislit. The interference filter was

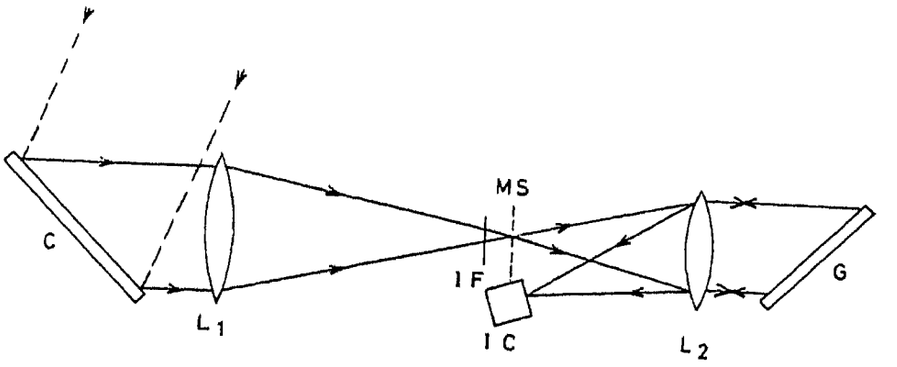

Fig. 1: Experimental set up for high resolution spectroscopy in 6374 Å line. C = coelostat mirror; L_1 = objective (ϕ = 140 mm, f = 1400 mm); IF = interference filter; MS = multislit; L_2 = collimator (ϕ = 100 mm, f = 1000 mm); G = grating (600 lines mm^{-1}); IC = image tube.

tilted to avoid an unwanted fringe pattern in the spectra and to shift the wavelength of peak transmission to around 6374 Å. The spacing between the slits, each 80 micron wide, was chosen to be 5 mm on the basis of the pass band of the interference filter and the dispersion of the spectrograph. In the Littrow focal plane, five spectra originating from the multi-slit each about 10 Å in width were stacked side by side on the photo cathode of a single stage Varo image intensifier. The image intensifier had a gain of 20 and an effective aperture of 30 mm which permitted the spectra to be recorded upto 2 $R_\odot$ from the sun's centre. A plate holder magazine enabled a quick change-over of the emulsion that had to be in contact with the fibre optic face plate. The plate holder could be loaded with six plates at a time. Each spectrum had also a neon comparison. Since these spectral lines were not filtered by the interference filter, lines from overlapping orders were also recorded and this permitted multiple checks on the velocity measurements. With a view to estimating the exposure time to be used at the time of eclipse, spectra of the moon light near full moon were obtained. The spectral quality was found to be excellent.

2.3. Observations

Two of the three plates exposed during the total phase of the eclipse have been used in this study. The first exposure was discarded because of excessive tube background intensity that had accumulated by virtue of the hot afternoon and the fact that the tube had been turned on several minutes before totality so as to be in readiness for the event. The exposures used were both of 45 s duration and enabled the detection of the emission lines to distances as far as 1.7 $R_\odot$. Between the first and second exposures, the solar image was shifted through 4.5 arcmin along the axis of solar rotation in order to sample a new set of coronal regions with the multislit. We call these positions 1 and 2. Thus plate 1 contains the spectra with the multislit in position 1 and plate 2 those of position 2 of the multislit. The two spectra obtained in the two positions are shown in Figures 2 and 3. The spectra were exposed on Eastman 103a-D emulsion and developed in D-19 at a temperature of 20 C for five minutes together with the step wedge calibration obtained immediately after the eclipse with the same spectrograph. Neon spectra obtained along the entire length of the four slits permitted the evaluation of the instrumental line profiles at several points on

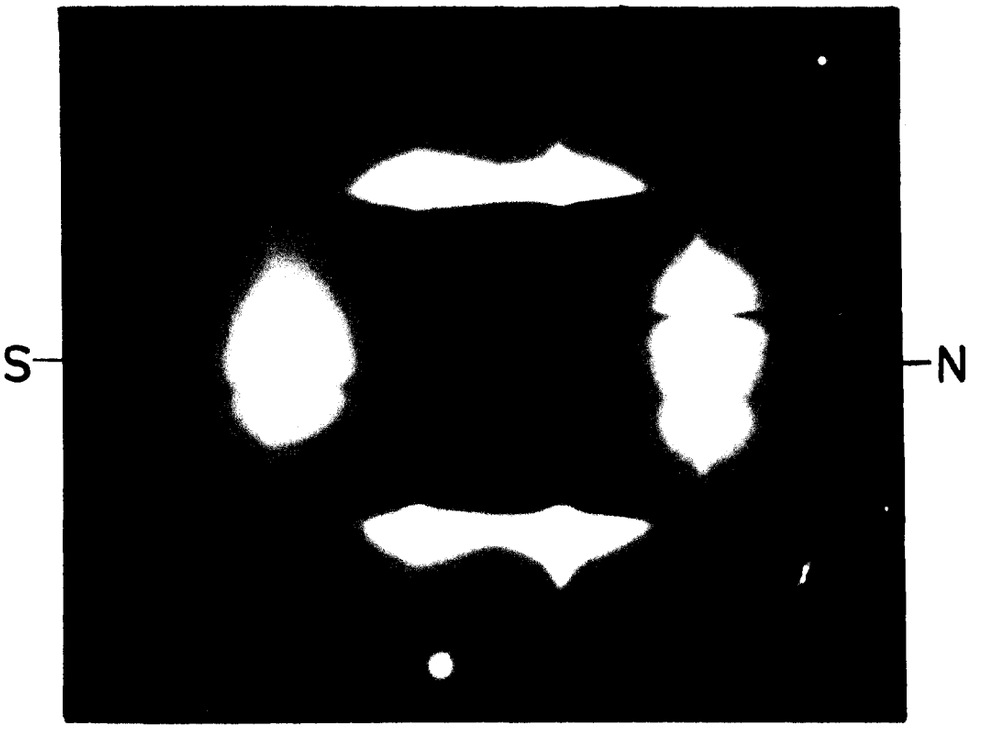

Fig.2: Spectra of 6374 Å line of eclipse of February 16, 1980 with the multislit in position 1. Exposure = 45 s. N-S represents the rotation axis of the sun.

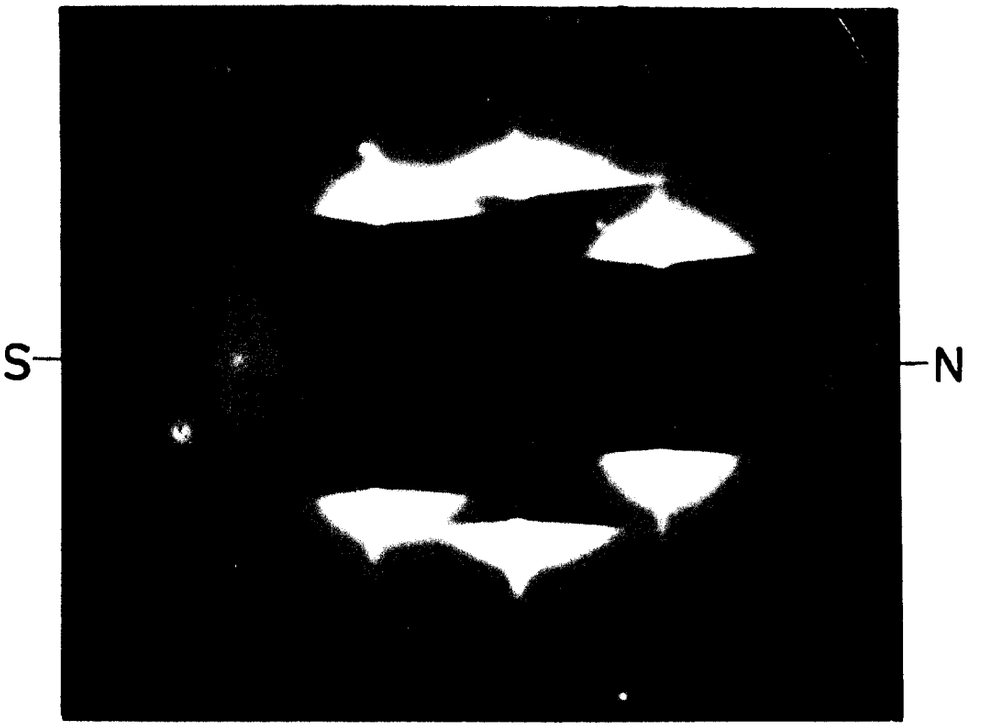

Fig.3: Spectra of 6374 Å line of eclipse of February 16, 1980 with multislit in position 2, which is 4.5 arcmin away from position 1. Exposure = 45 s. N-S represents the rotation axis of the sun.

each slit. We show in Figure 4 the values of the full width at half maximum (FWHM) of these instrumental line profiles at several points on each slit and the final mean value assigned to each which was used in the determination of the coronal line widths.

We obtained microphotometer scans of these spectra with a projected slit size of 4.5 x 22 arcsec^2 on the plate. Successive scans were separated by 30 arcsec along the slit. This spacing had to be increased to 45 or 50 arcsec at locations where the ratio of maximum line intensity to continuum intensity was low. The transmission curve of the narrow interference filter was evaluated with the aid of the solar spectrum and the Kodaikanal 18 m spectrograph. Working at a dispersion of 7.4 mm $\mathring{A}^{-1}$, transmission spectra through several different regions of the interference filter, each spaced 5 mm from its neighbour, were used for the evaluation of the mean filter characteristic (Figure 5). The normalized mean transmission curve of the filter thus obtained was used to operate on the intensity curve of the red coronal line, as evaluated at each point along the slit (Figure 6). This procedure gave the observed profile of the coronal line. The FWHM was corrected for instrumental line width using the data of Figure 4 and the assumption that both profiles

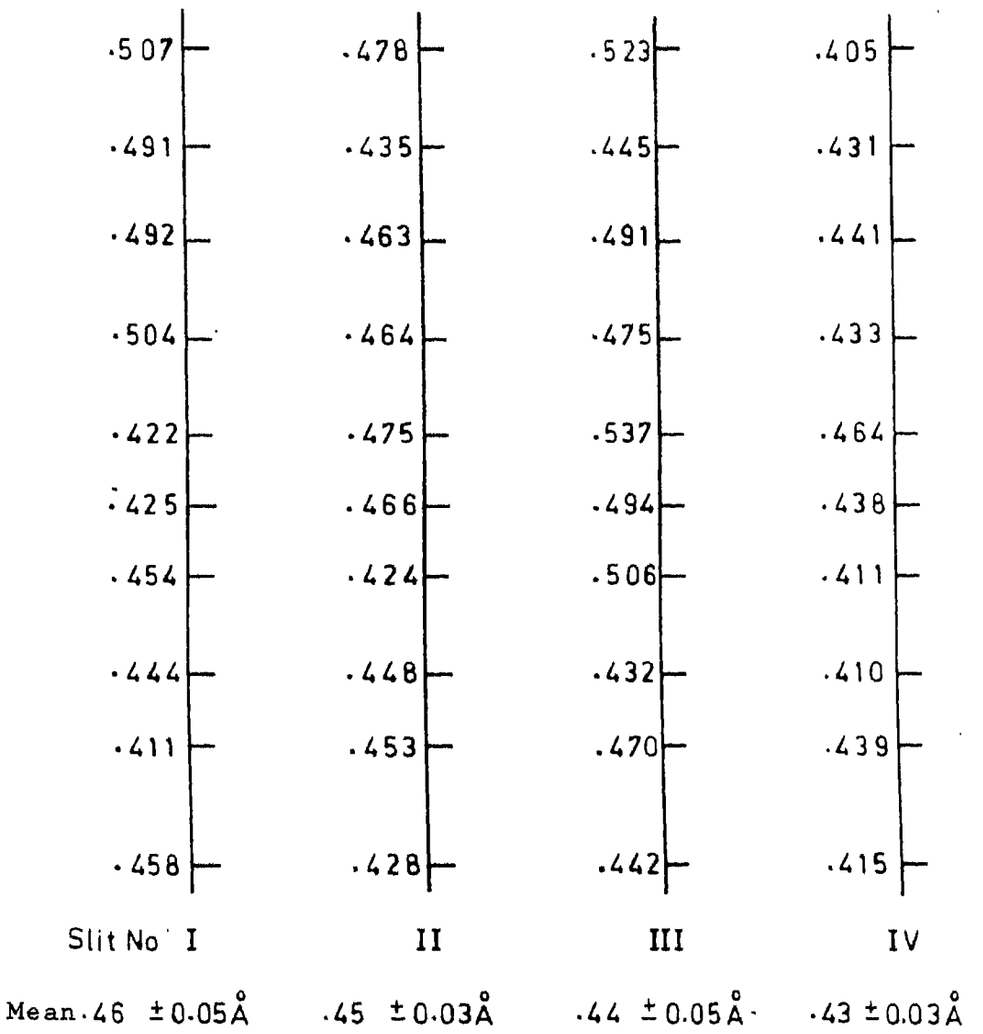

Fig. 4: Full width at half maximum of the instrumental line profile at various locations along the slits. Mean value is indicated below each slit.

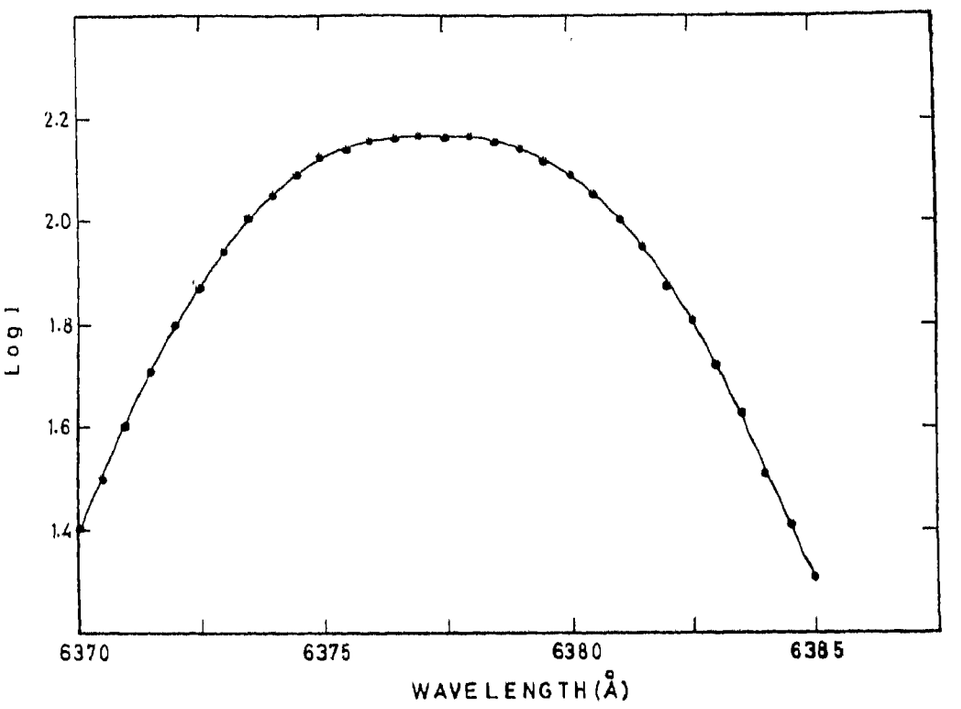

Fig. 5: Mean transmission curve of the interference filter.

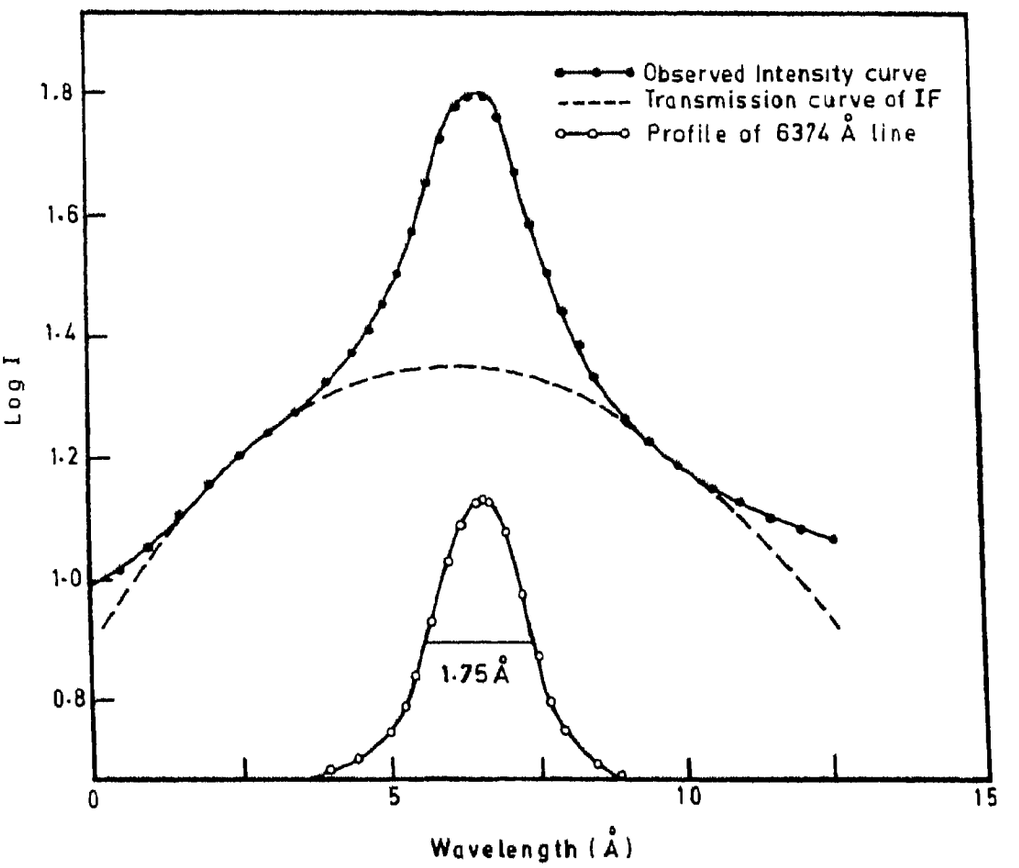

Fig. 6: A typical line profile of 6374 Å at one of the locations within the corona. Above full line represents a plot of log I vs wavelength. The dotted line represents the transmission curve of the interference filter on the same scale. Shown below is the line profile plotted as intensity vs wavelength, after correcting for the transmission through the interference filter.

are Gaussian. The true width is given by

$$(FWHM)_{true} = \left[(FWHM)^2_{obs} - (FWHM)^2_{Inst}\right]^{\frac{1}{2}} \quad .. \quad (2.1)$$

Image tube spectra suffer from the pin-cushion effect of the image intensifier and, therefore, require precautions to be taken in radial velocity measurements. To free the data from the uncertainties of the pin-cushion effect, the following steps were adopted. A cross wire placed on the slits served as a local fiducial reference for all measurements. The [Fe X] line was flanked on either side by the neon lines 8495.36 Å of the third order (equivalent to 6371.52 Å of the fourth order) and 6382.99 Å of the fourth order. The wavelength of [Fe X] line was evaluated at every 30 arcsec along each slit by interpolating between these two neon lines for each location. We assume that the differential pin-cushion effect between the two neon lines which are close to each other is insignificant and would not affect our measurements. In addition the entire spectra were confined to the central portion of the image tube where the pin-cushion effect is the least.

2.4. Results

The red coronal line widths were measured at 236 locations in the solar corona. These range from 1.1 $R_\odot$

to 1.7 $R_\odot$ and give a satisfactory coverage all around the solar limb. The data are presented in Table 3. The position angle measured from the north point of the projected axis of solar rotation and the radial distance from the centre of the disc are given in columns 2 and 3. The values of FWHM are in column 4 while column 5 gives the turbulent velocities derived by assuming the temperature of the corona to be 1.3×10^6K. Column 6 contains the equivalent temperature if the FWHM is ascribed entirely to thermal broadening. Columns 7 and 8 give the peak brightness of the continuum at the wavelength of the line centre as well as the peak brightness of the line. This is expressed as a ratio in column 9 and serves to portray the localized enhancement of the line emission over that of the background K-corona.

The derived values of FWHM of the red coronal line lie between 0.6 Å and 2.4 Å. These values for different locations are depicted in Figure 7. In this Figure, the positions of the four slits on the solar image on plate 1 are represented by I(1), II(1), III(1) and IV(1) and those on plate 2 by corresponding designations with suffix 2 in brackets. We have superposed on these a schematic hand sketch of the most conspicuous features in the corona as seen in the white

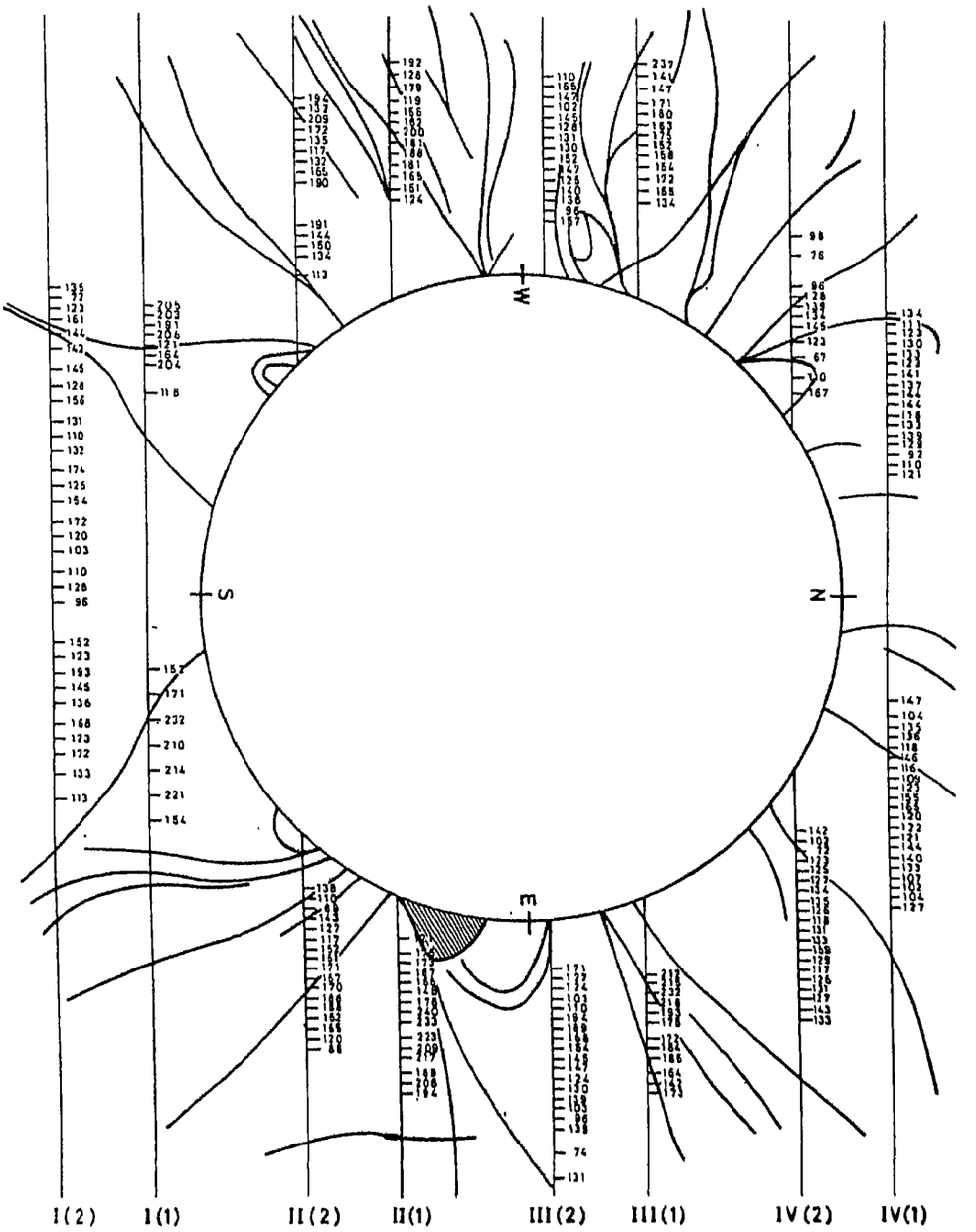

Fig. 7: I(1), II(1), III(1) and IV(1) represent the slit positions on the solar disc on plate 1 and the corresponding designations with suffix 2 in bracket represent those on plate 2. The numbers indicate the true line widths of the 6374 Å line at various locations in units of Å x 10^{-2}. A free hand sketch of the conspicuous features of the corona as seen in the white light photograph is superposed to help relate the line width values with the coronal features. Shaded area on E-limb stands for an enhancement.

light photograph to enable us to relate the line width values with the coronal forms. The plot of the histogram of the line widths (Figure 8) shows a predominance of values of FWHM around 1.3 Å and an extended tail towards higher values. In Figure 9, we have plotted line widths vs radial distance, and this shows that the line widths are randomly distributed and do not have any maximum value at any particular radial distance. The mean curve of all these plots is shown in Figure 10 and this does indicate a line width maximum around the radial distance of 1.4 $R_\odot$.

Line and continuum intensities

Our measures of intensity, both at the peak of the line and the underlying continuum, can be used for the study of the intensity gradients of both the emission corona and the K-corona. The multislit arrangement covers several helmets and streamers and it is possible to choose those locations where the slit has an almost radial orientation. Such locations are contained along the slit in positions II(2) and III(1) in the west and in positions III(2) and IV(2) in the east. In Figure 11 we plot the logarithms of the intensity of the K-corona and of the emission corona against radial distance for these locations and obtain gradients of intensity. The crosses indicate the

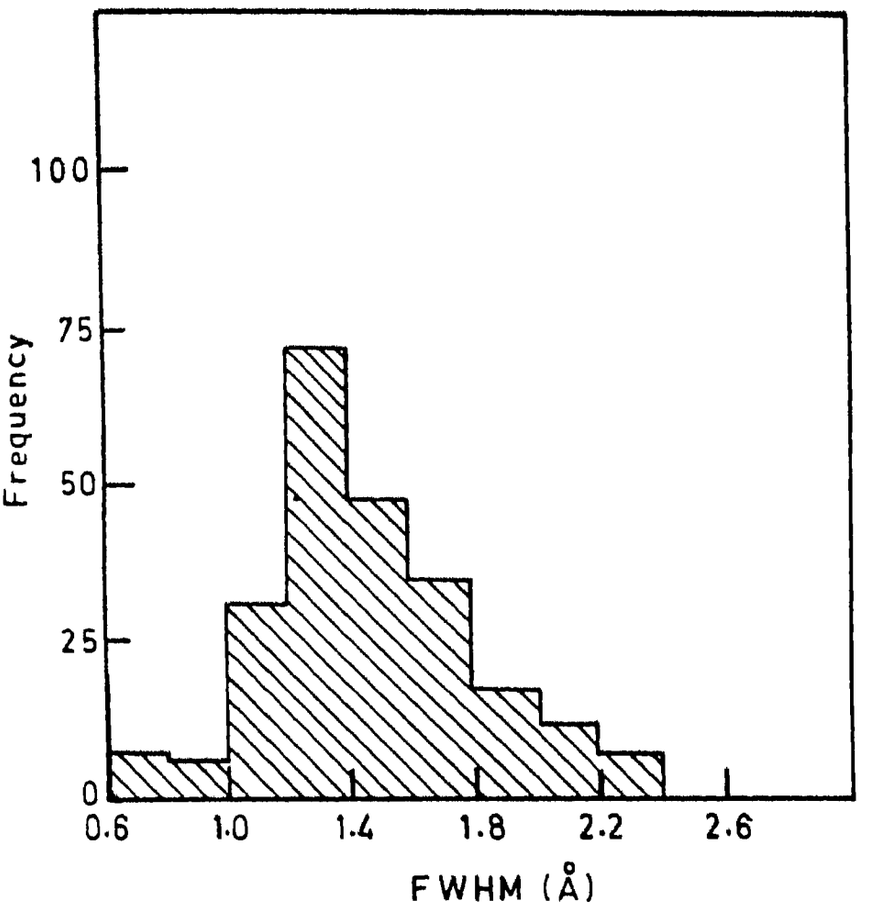

Fig. 8: Frequency distribution of the true line widths of 6374 Å.

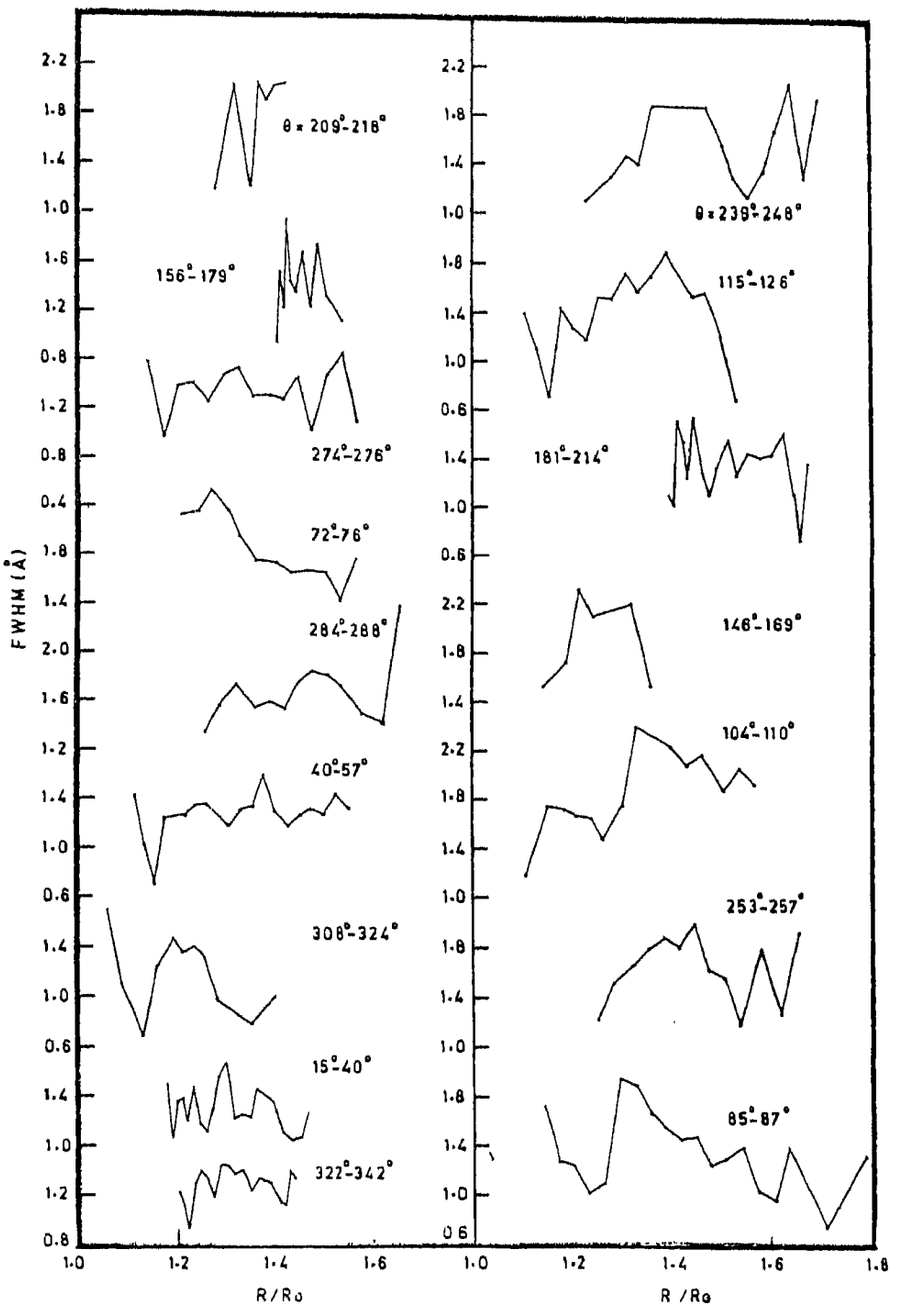

Fig. 9: Variation of the true line widths with radial distance. Position angle for each direction is also indicated.

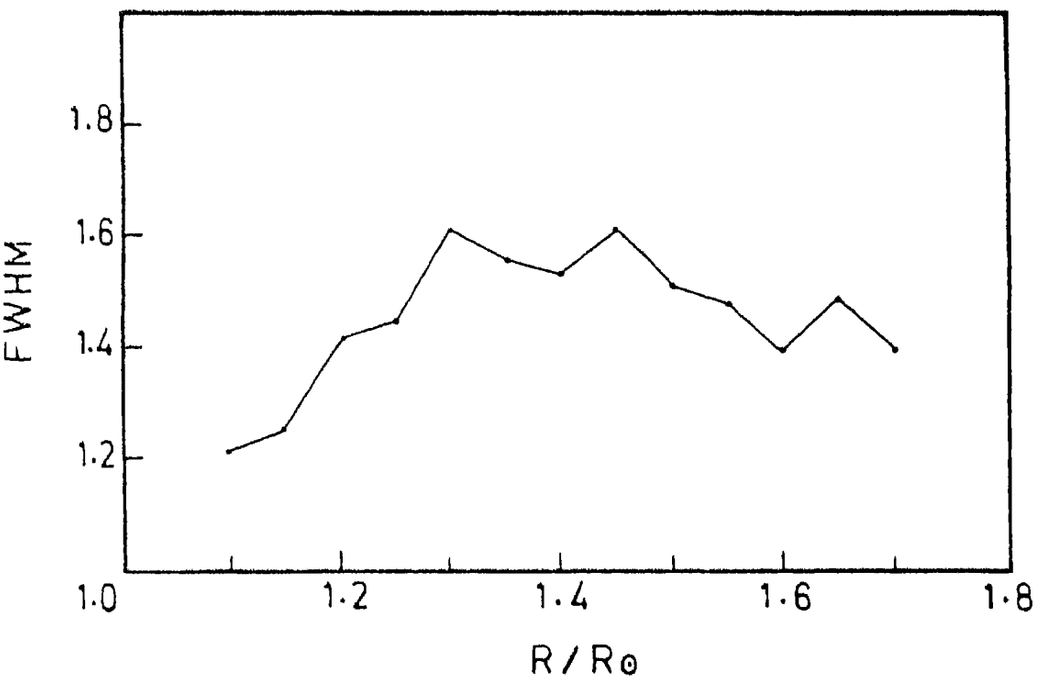

Fig. 10: Mean variation of the line width with radial distance.

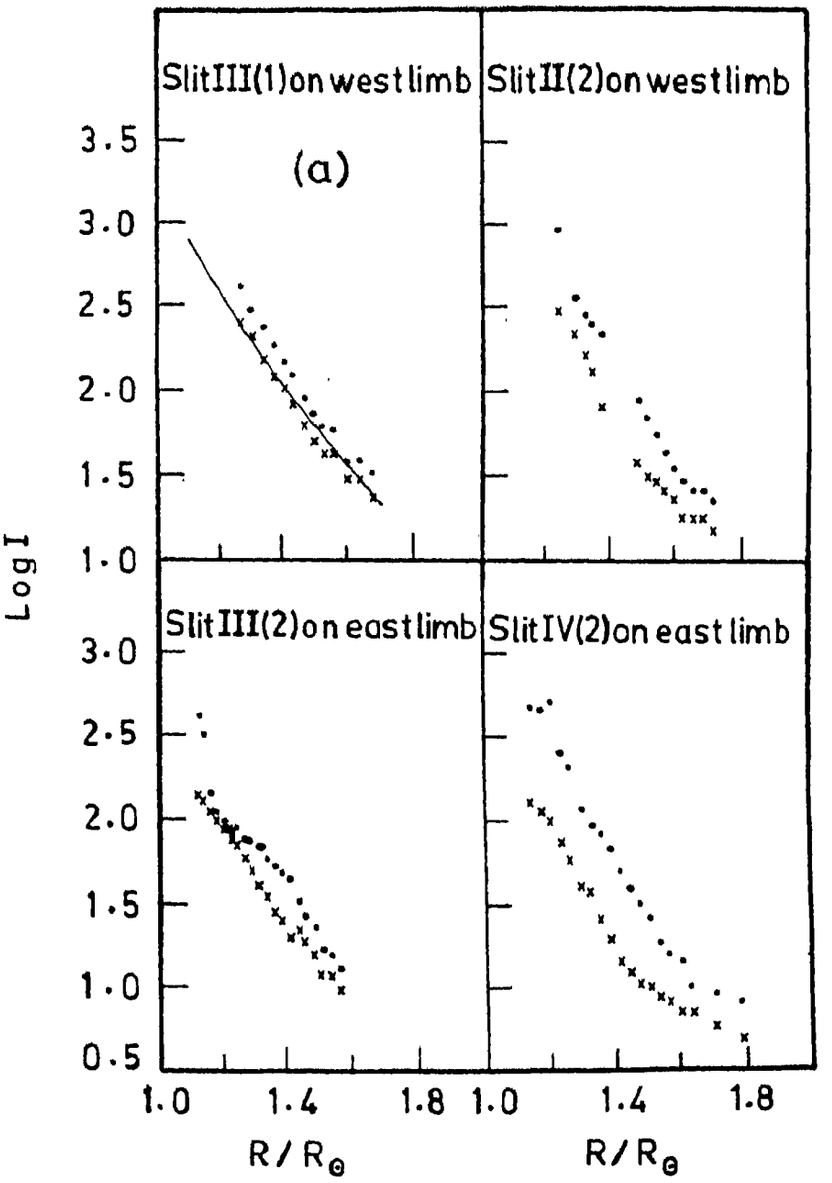

Fig. 11: Intensity of continuum (crosses) and 6374 Å line (filled circles) in logarithmic units vs radial distance. The full line in box (a) is the intensity gradient obtained by Sivaraman et al. (1984) for the K-corona.

brightness of the K-corona and filled circles that of the 6374 Å line. The brightness distribution in the corona for values of $R/R_\odot$ reaching 2.5 has been derived at this eclipse by a team from the Indian Institute of Astrophysics. We have compared these gradients determined by Sivaraman et al. (1984) in absolute units of intensity with our values obtained from the multislit. We have matched the two curves at the intensity level corresponding to 1.4 $R_\odot$. We have plotted in box (a) of Figure 11 the intensity gradients obtained from the broad band photographs by Sivaraman et al. (1984) for equatorial region in solid line and we find the gradients obtained by us matches well with these.

The mode of excitation of the lines can be indirectly understood from the behaviour of the line intensity (I_l) and the continuum intensity (I_c) as a function of the radial distance. For this purpose we have plotted the ratio (I_l/I_c) versus radial distance for all those directions for which the data were available. These plots are distributed in two Figures 12 and 13 depending upon their behaviour. Figure 12 shows that I_l/I_c is almost constant with radial distance between 1.2 $R_\odot$ and 1.4 $R_\odot$. Figure 13 indicates that I_l/I_c falls steeply till 1.2 $R_\odot$ and

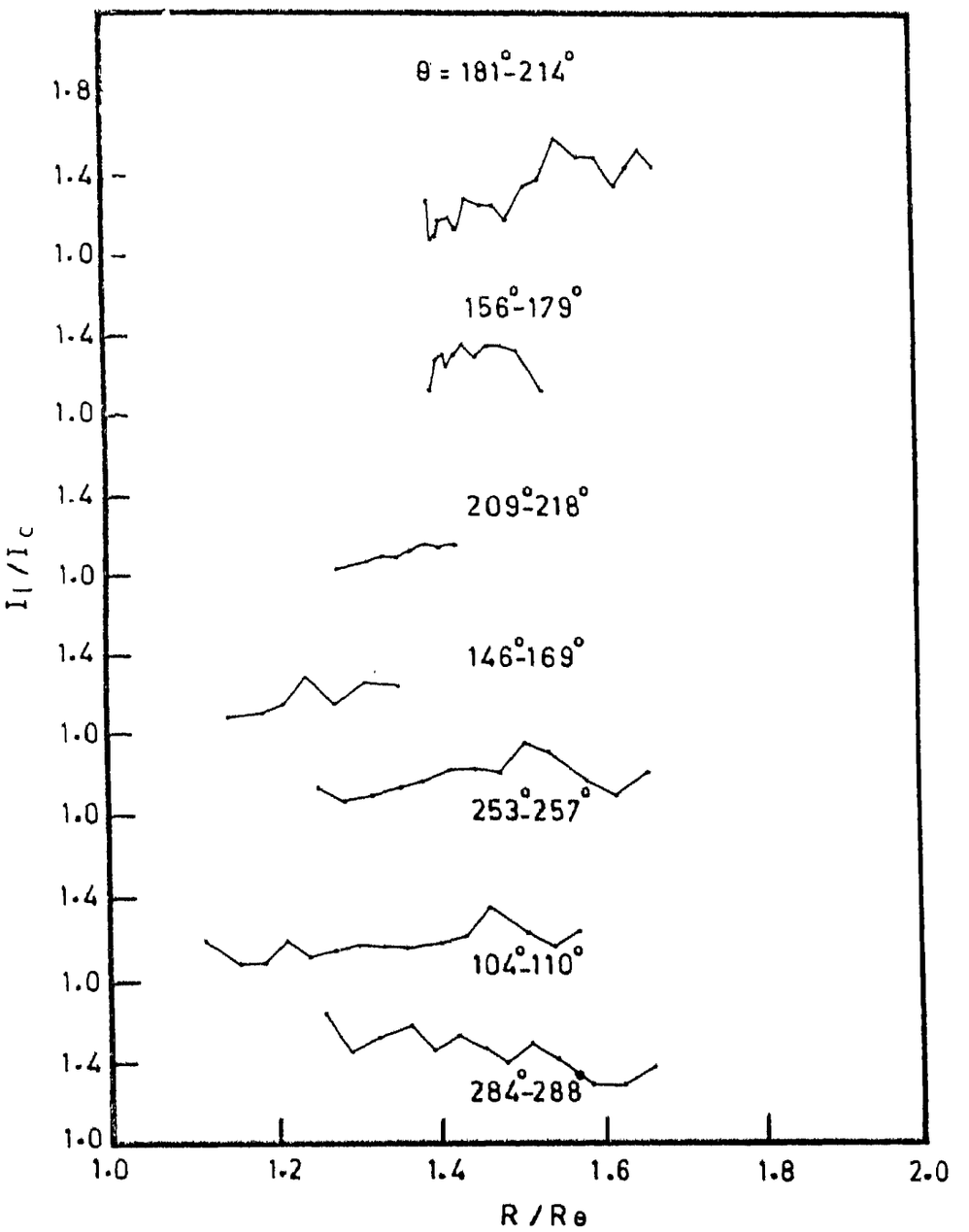

Fig. 12: I_1/I_c vs radial distance. Position angle in degrees is indicated for each curve.

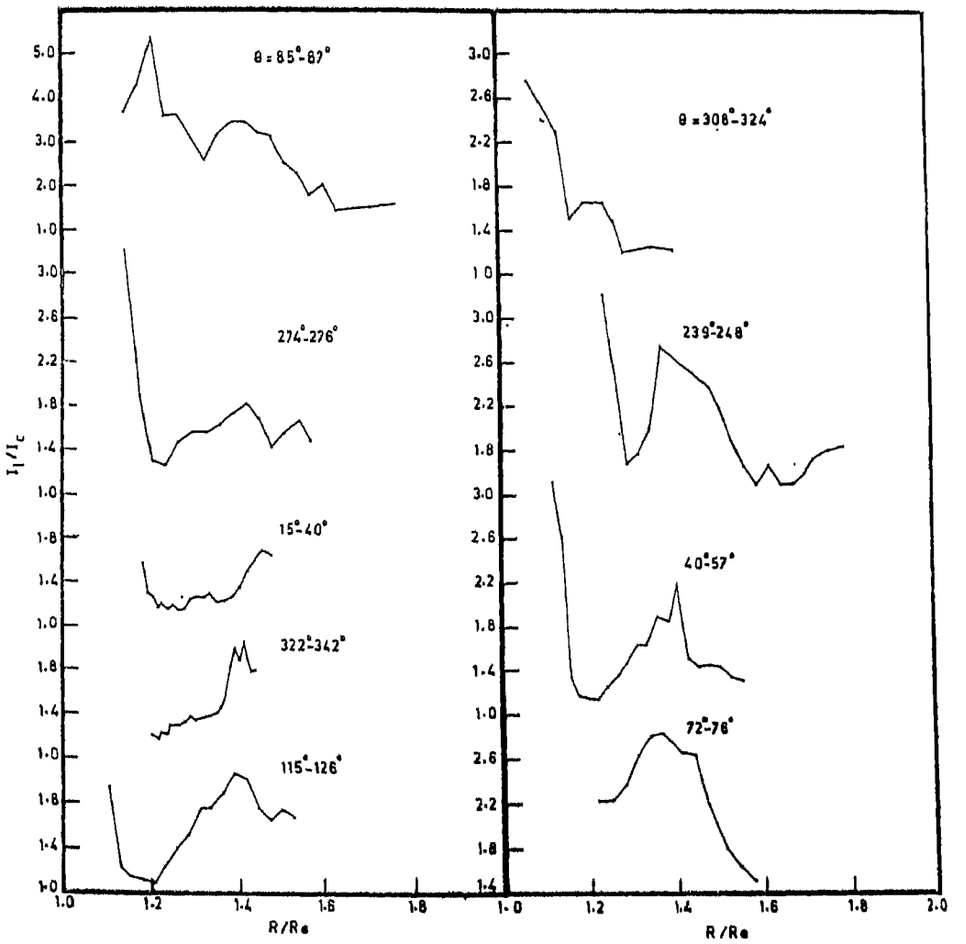

Fig. 13: I_1/I_c vs radial distance. Position angle in degrees is indicated for each curve.

rises subsequently with a maximum around 1.4 $R_\odot$. The ratio I_1/I_c^2 as a function of radial distance, for all those directions for which data were available, is shown in Figures 14 and 15. Only four directions, out of all these 16 directions, have data points between 1.1 and 1.2 $R_\odot$. These four plots indicate that the ratio I_1/I_c^2 remains almost constant upto 1.2 $R_\odot$. But all the 16 plots show that this ratio increases with radial distance beyond 1.2 $R_\odot$. The gradient is rather slow between 1.2 and 1.4 $R_\odot$ but increases beyond 1.4 $R_\odot$. The inferences of this behaviour are discussed in Chapter 5. In this context it may be worthwhile to look at the relationship between the line width and I_1/I_c^2 obtained by Desai and Chandrasekhar (1983). Their plot of I_1/I_c^2 versus line width temperature is reproduced in Figure 16. A least square straight line and parabola fitted into these data points by them are also shown. They find a negative correlation co-efficient of 0.53 between this ratio and line width temperature. A similar plot (Figure 17) for our data for the same eclipse does not indicate any relationship between the two quantities. The reason for this is as follows. The observed line width contains the contribution from thermal as well as nonthermal motions of the ions but the relative contribution of each is

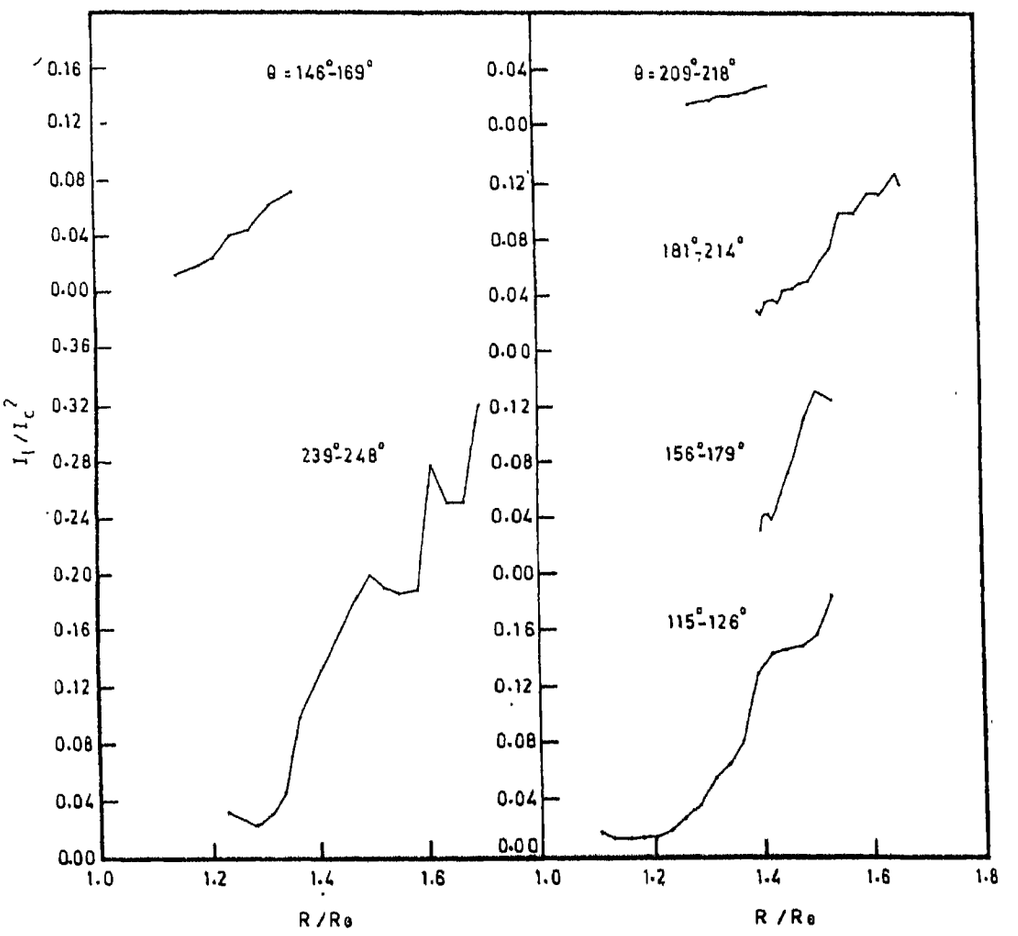

Fig. 14: I_1/I_c^2 vs radial distance. Position angle in degrees is indicated for each curve.

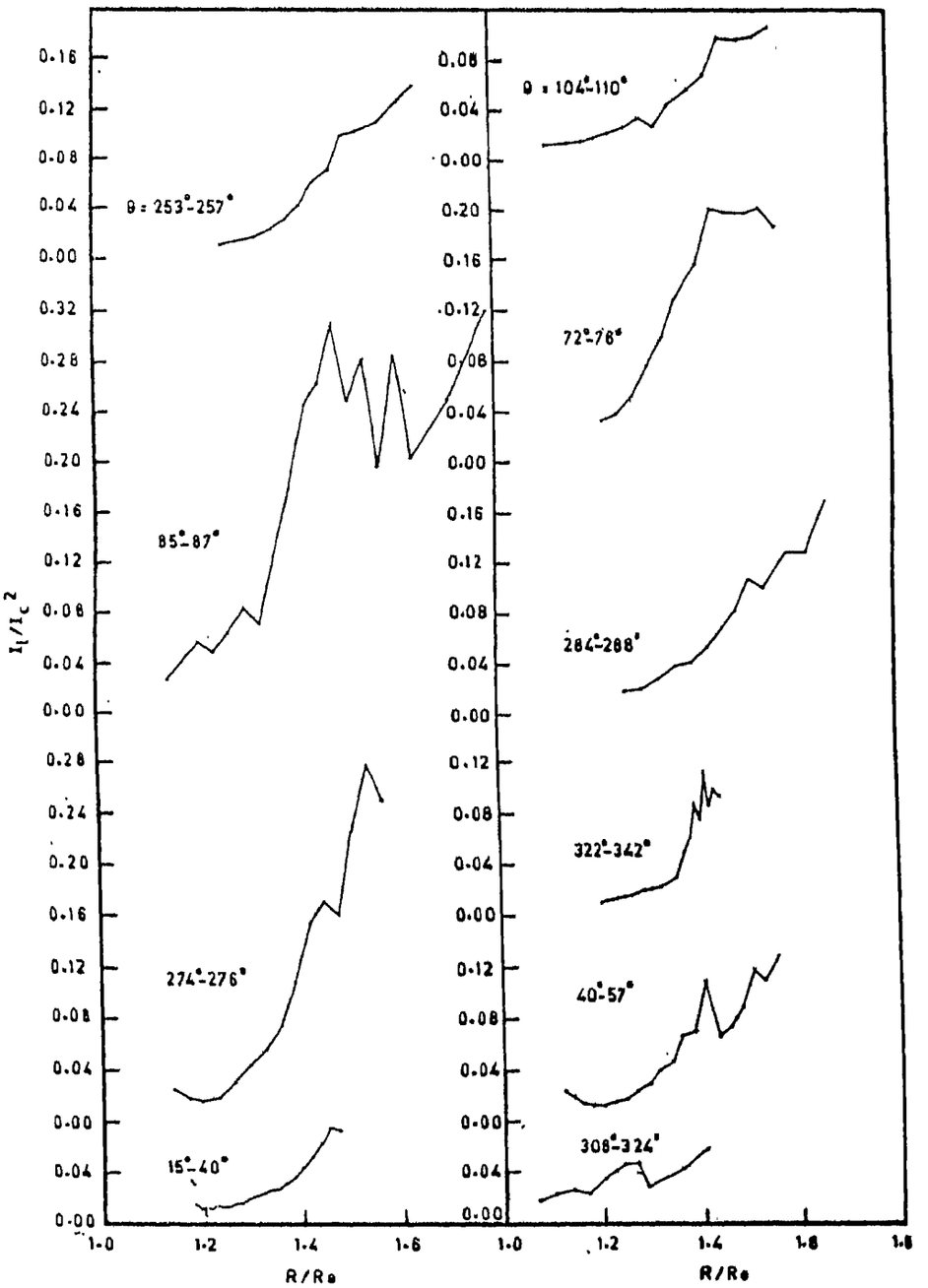

Fig. 15: I_1/I_c^2 vs radial distance. Position angle in degrees is indicated for each curve.

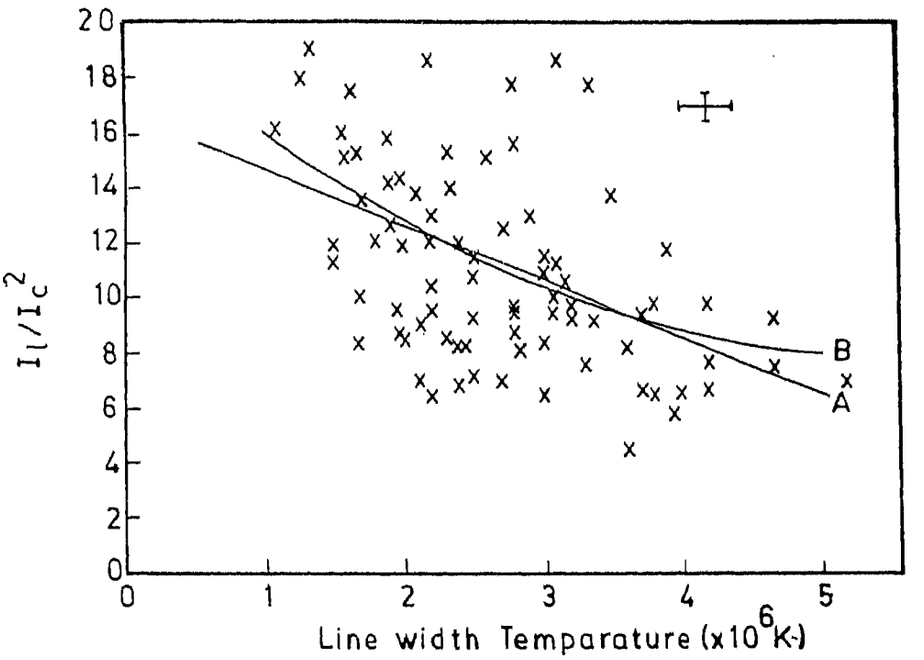

Fig. 16: I_1/I_c^2 plotted against line width temperatures. A = linear fit with a correlation coefficient of 0.52, B = quadratic fit with a correlation coefficient 0.53 (Desai and Chandrasekhar 1983).

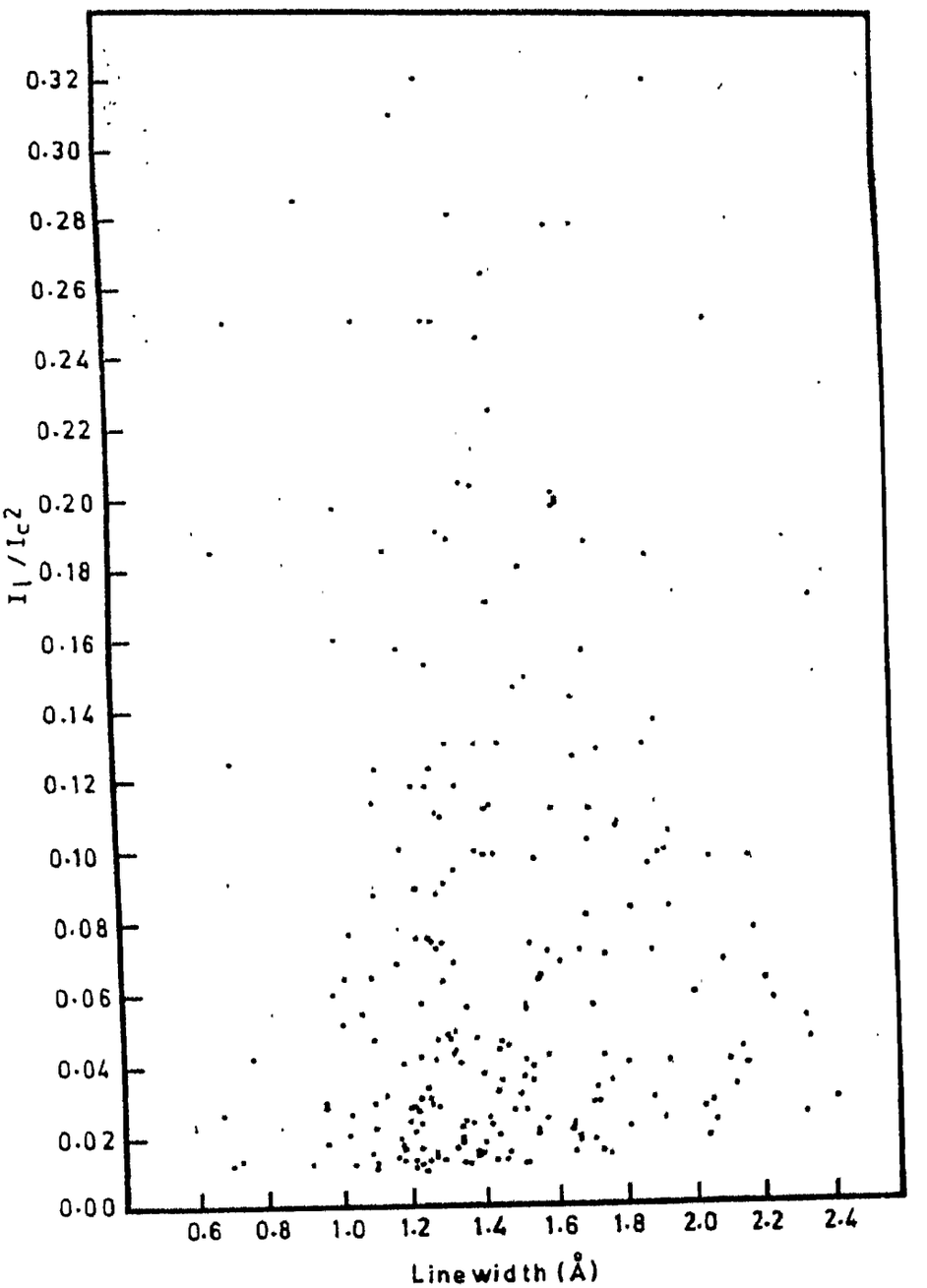

Fig. 17: The ratio I_1/I_c^2 vs line width.

not fully known. Also the variation of line intensity with continuum intensity is not uniform. For pure collisional excitation I_1/I_c^2 will be constant and for pure radiative excitation I_1/I_c will be constant. Since both collisional as well as radiative excitations are important in the solar corona, as will be discussed in Chapter 5, it may not be reasonable to expect any definite relationship between line width and I_1/I_c^2.

Coronal hole

The presence of a conspicuous coronal hole near the south pole was one of the striking features of the 1980 eclipse. We have several measures that cover the position angle range 170-190°. The tangential slit position restricts the $R/R_\odot$ values between 1.43 and 1.53. A noticeable characteristic of the line widths is that a majority of them have small values. We interpret this to mean that the random motions sampled in this region in the line of sight are of small magnitude.

Line-of-sight velocities in the corona and coronal equatorial rotation

Radial velocities were measured at several points along each slit on both the east and west corona, with the aid of the neon comparison lines. These values

are shown in Table 4 and refer to the solar equator. The slit positions II(1), III(2) and III(1) have been utilized for deriving the rotation. The scatter amongst the several different values of the displacement of the coronal emission line lowers the accuracy of our measurement. This is unlike the measures from absorption lines of photospheric origin. We have, therefore, grouped for each slit position the east and the west values. The mean wavelength of the line (6374.596 $\pm$ 0.02 Å) derived from the measures near the north and south poles serves as the zero reference for calculating the rotation. The coronal rotation thus derived has a value of 2.6 kms^{-1} and is comparable to the photospheric value. The limited accuracy of our measures (probable error $\pm$ 1.5 kms^{-1} of the faint broad lines only permits a confirmation of corotation of the corona.

With these limited data it is not possible to study the variation of rotation rate with height and latitude. Trellis (1957), using successive east and west limb passages of bright 5303 Å features, determined the coronal rotation rate for each latitude from 0 to 70°. He concluded that the corona rotated a little more slowly than the photosphere at latitude below 35°, and more rapidly above 35°. Waldmeier (1950)

obtained a rotation rate from the observations of a single emission feature at 55° that maintained its identity for almost seven rotations. The rate he found was significantly higher than the 55° rate on the curve determined by Trellis. Cooper and Billings (1962) observed an emission region at 65° for 29 successive rotations and found a rotation rate that was in excess of that found by either Waldmeier or Trellis. Since these emission features are connected with active zone features of photosphere by strong magnetic fields and hence are likely to show a rotation rate comparable to photospheric rotation rate. On the other hand the present measures are independent of the emission features and give a rotation rate comparable to that of photosphere.

A distribution of the line-of-sight velocities measured all over the corona is shown in Figure 18. None of the regions covered by the slits show any abnormally large velocities in the corona as claimed earlier by Delone and Makarova (1969) and for this eclipse by Desai, Chandrasekhar and Angreji (1982). The latter also find a splitting of the interference fringe pattern at P.A. 256° indicating a component

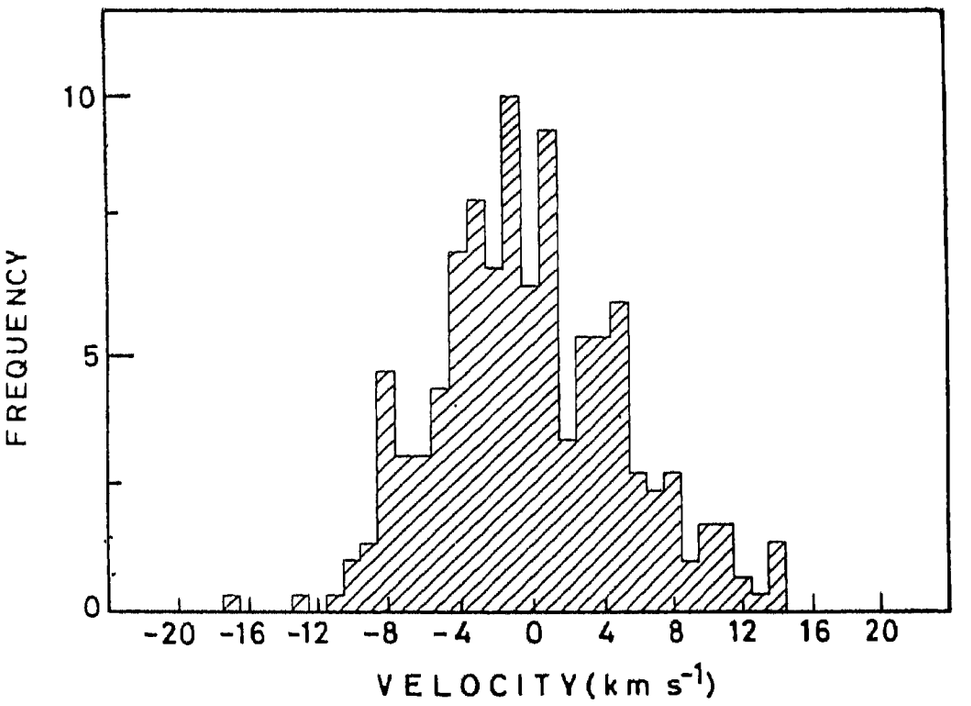

Fig. 18: Frequency distribution of line-of-sight velocities as derived from 6374 Å line.

with a line-of-sight velocity of about 70 kms^{-1}. This, if confirmed, would imply that there is a mass component with a velocity indicating expansion in perhaps a preferred direction. This region is covered by our slit position II(1) that spans the position angle 252-257°. We neither see any splitting of the emission line, nor find any abnormal velocity even of the line as a whole. The observed velocities are all within the range of $\pm$ 11 kms^{-1}. However, one should note that we have derived the line-of-sight velocities from the red coronal line sensitive to a region with temperature of 1.3×10^6 K whereas Desai, Chandrasekhar and Angreji (1982) have used the green line emitted mostly from regions with a temperature of 2.3×10^6 K.

Table 3

Line widths, intensities and turbulent velocities derived from the red coronal line

No.	Position angle θ	$R/R_\odot$	FWHM Å	V_t Kms^{-1}	$T \times 10^{-6}$	I_c	I_l	$\frac{I_l}{I_c}$
1.	2.	3.	4.	5.	6.	7.	8.	9.
			Slit IV (1)					
1	322.9	1.437	1.34	29	4.8	19	34	1.79
2	323.4	1.428	1.40	32	5.3	18	32	1.78
3	323.9	1.418	1.11	19	3.3	22	42	1.91
4	324.4	1.409	1.12	20	3.4	19	41	2.16
5	324.9	1.400	1.23	25	4.1	25	47	1.88
6	325.4	1.391	1.29	28	4.5	23	46	2.00
7	325.9	1.382	1.30	28	4.6	29	53	1.83
8	327.0	1.365	1.33	29	4.8	31	47	1.52
9	328.1	1.349	1.23	25	4.1	47	66	1.40
10	329.2	1.332	1.41	32	5.3	54	74	1.37
11	330.3	1.317	1.37	30	5.1	59	80	1.36
12	331.5	1.301	1.44	33	5.6	67	90	1.34
13	332.7	1.287	1.44	33	5.6	68	93	1.37
14	333.9	1.273	1.18	23	3.8	77	102	1.32
15	335.2	1.259	1.33	29	4.8	81	105	1.30
16	336.5	1.246	1.39	31	5.2	83	107	1.29
17	337.8	1.234	1.29	27	4.5	91	111	1.22
18	339.1	1.222	0.92	9	2.3	98	119	1.21
19	340.5	1.212	1.10	19	3.3	101	118	1.17
20	341.8	1.202	1.21	24	4.0	105	125	1.19
21	40.0	1.475	1.27	26	4.4	22	36	1.64
22	39.1	1.456	1.04	17	2.9	22	37	1.68
23	38.1	1.437	1.02	15	2.8	25	40	1.60
24	37.1	1.418	1.07	18	3.1	28	42	1.50
25	36.1	1.400	1.33	29	4.8	31	42	1.35
26	35.1	1.383	1.40	31	5.3	34	43	1.26
27	34.0	1.365	1.44	33	5.6	39	48	1.23
28	32.9	1.349	1.21	24	3.9	43	52	1.21
29	31.8	1.332	1.22	25	4.0	48	62	1.29
30	30.7	1.317	1.20	24	3.8	53	67	1.26

Table 3 - continued

1.	2.	3.	4.	5.	6.	7.	8.	9.
31	29.5	1.302	1.65	40	7.4	57	72	1.26
32	28.3	1.287	1.55	36	6.5	62	77	1.24
33	27.1	1.273	1.23	25	4.1	74	85	1.15
34	25.8	1.259	1.09	19	3.2	79	91	1.15
35	24.5	1.247	1.16	22	3.7	85	100	1.18
36	23.2	1.234	1.46	33	5.7	89	102	1.15
37	21.9	1.223	1.18	23	3.8	94	113	1.20
38	20.5	1.212	1.36	30	5.0	96	111	1.16
39	19.2	1.202	1.35	29	4.9	106	132	1.25
40	17.8	1.192	1.04	17	2.9	108	140	1.30
41	15.6	1.179	1.47	34	5.8	107	168	1.57
			Slit IV (2)					
42	308.4	1.403	0.98	13	2.6	21	26	1.24
43	310.0	1.355	0.76	1	1.5	30	38	1.27
44	312.6	1.285	0.96	12	2.5	43	52	1.21
45	313.5	1.263	1.28	27	4.4	32	48	1.50
46	314.5	1.240	1.39	31	5.2	35	58	1.66
47	315.5	1.218	1.34	29	4.8	41	68	1.66
48	316.5	1.197	1.45	33	5.7	47	78	1.66
49	318.2	1.165	1.23	25	4.1	65	99	1.52
50	319.9	1.134	0.67	0	1.2	90	207	2.30
51	322.4	1.096	1.10	19	3.3	116	299	2.58
52	324.3	1.068	1.67	40	7.6	148	407	2.75
53	56.8	1.553	1.33	29	4.8	10	13	1.30
54	56.2	1.528	1.43	32	5.5	12	16	1.33
55	55.5	1.502	1.27	26	4.4	12	17	1.42
56	54.8	1.477	1.31	28	4.6	16	23	1.44
57	54.1	1.452	1.26	26	4.3	19	27	1.42
58	53.4	1.428	1.17	22	3.7	22	33	1.50
59	52.6	1.403	1.29	27	4.5	20	44	2.20
60	51.8	1.379	1.59	38	6.8	26	48	1.85
61	51.0	1.355	1.33	29	4.8	28	53	1.89
62	50.2	1.332	1.31	28	4.6	35	57	1.63
63	49.3	1.308	1.18	23	3.7	41	67	1.63
64	48.4	1.285	1.26	26	4.3	50	73	1.46
65	47.5	1.263	1.35	29	4.9	57	77	1.35

Table 3 - continued

1.	2.	3.	4.	5.	6.	7.	8.	9.
66	46.5	1.240	1.34	29	4.8	71	89	1.25
67	45.5	1.218	1.27	26	4.4	77	87	1.13
68	44.5	1.197	1.25	26	4.2	86	98	1.14
69	43.4	1.176	1.23	25	4.1	96	112	1.17
70	42.3	1.155	0.72	0	1.4	108	146	1.35
71	41.1	1.135	1.02	15	2.8	125	327	2.62
72	39.9	1.115	1.42	32	5.5	137	426	3.11
			Slit III (1)					
73	283.9	1.660	2.37	62	15.1	8	11	1.38
74	284.2	1.623	1.41	32	5.3	10	13	1.30
75	284.5	1.586	1.47	34	5.8	10	13	1.30
76	285.0	1.541	1.71	42	7.0	14	20	1.43
77	285.3	1.511	1.80	45	8.7	14	21	1.50
78	285.6	1.481	1.83	46	9.1	17	24	1.41
79	285.9	1.452	1.75	43	8.3	21	31	1.48
80	286.2	1.422	1.52	35	6.3	28	43	1.54
81	286.5	1.393	1.58	37	6.7	35	51	1.46
82	286.9	1.363	1.54	36	6.4	41	65	1.59
83	287.4	1.326	1.72	42	8.0	53	81	1.53
84	287.9	1.289	1.55	36	6.5	71	104	1.46
85	288.3	1.260	1.34	29	4.8	85	140	1.65
86	76.3	1.571	1.73	42	8.1	8	12	1.50
87	76.0	1.541	1.42	32	5.4	8	13	1.63
88	75.8	1.511	1.64	40	7.3	9	16	1.78
89	75.3	1.467	1.65	40	7.4	11	24	2.18
90	75.0	1.437	1.64	40	7.3	13	34	2.62
91	74.6	1.407	1.72	42	8.0	17	45	2.65
92	74.1	1.363	1.75	43	8.3	22	62	2.82
93	73.7	1.334	1.93	49	10.1	28	78	2.79
94	73.3	1.304	2.18	57	12.8	34	89	2.62
95	72.9	1.275	2.32	61	14.5	45	106	2.36
96	72.5	1.245	2.15	56	12.5	57	127	2.23
97	72.1	1.216	2.12	55	12.2	68	151	2.22

Table 3 - continued

1.	2.	3.	4.	5.	6.	7.	8.	9.
			Slit III (2)					
98	274.4	1.573	1.10	19	3.3	6	9	1.50
99	274.5	1.542	1.65	40	7.4	6	10	1.67
100	274.6	1.511	1.47	34	5.8	7	11	1.57
101	274.7	1.481	1.02	15	2.8	9	13	1.44
102	274.8	1.450	1.45	33	5.7	10	17	1.70
103	274.9	1.419	1.28	27	4.4	12	22	1.83
104	275.0	1.389	1.31	28	4.6	16	28	1.75
105	275.1	1.358	1.30	28	4.5	22	36	1.64
106	275.2	1.327	1.52	35	6.2	28	44	1.57
107	275.3	1.297	1.47	34	5.9	35	55	1.57
108	275.4	1.266	1.25	26	4.2	50	74	1.48
109	275.5	1.235	1.40	31	5.3	71	90	1.27
110	275.6	1.205	1.38	30	5.1	86	113	1.31
111	275.8	1.174	0.96	12	2.5	106	202	1.91
112	275.9	1.143	1.57	37	6.7	132	424	3.21
113	87.0	1.788	1.31	28	4.6	5	8	1.60
114	86.9	1.711	0.74	1	1.5	6	9	1.50
115	86.7	1.634	1.39	31	5.2	7	10	1.43
116	86.6	1.604	0.96	12	2.5	7	14	2.00
117	86.6	1.573	1.03	16	2.8	9	16	1.78
118	86.5	1.542	1.39	31	5.2	8	18	2.25
119	86.4	1.512	1.30	28	4.6	10	25	2.50
120	86.3	1.481	1.24	25	4.1	10	31	3.10
121	86.2	1.450	1.47	34	5.8	12	38	3.17
122	86.1	1.419	1.45	33	5.7	14	48	3.43
123	86.0	1.389	1.54	36	6.4	19	65	3.42
124	85.9	1.358	1.68	41	7.6	25	79	3.16
125	85.8	1.327	1.89	48	9.7	36	92	2.56
126	85.7	1.297	1.94	49	10.2	37	113	3.05
127	85.6	1.266	1.10	19	3.3	56	200	3.57
128	85.5	1.235	1.01	15	2.7	70	248	3.54
129	85.4	1.205	1.24	25	4.1	93	492	5.29
130	85.2	1.174	1.27	26	4.3	104	441	4.24
131	85.1	1.144	1.71	42	7.9	124	452	3.65

Table 3 - continued

1.	2.	3.	4.	5.	6.	7.	8.	9.
			Slit II (1)					
132	257.6	1.657	1.92	48	10.0	9	11	1.22
133	257.3	1.620	1.28	27	4.4	9	10	1.11
134	257.0	1.582	1.79	44	8.7	11	13	1.18
135	256.6	1.537	1.19	23	3.8	13	17	1.31
136	256.3	1.507	1.56	37	6.6	14	19	1.36
137	256.0	1.478	1.62	39	7.1	18	22	1.22
138	255.7	1.448	2.00	51	10.8	21	26	1.24
139	255.4	1.418	1.81	45	8.8	31	38	1.23
140	255.1	1.388	1.88	47	9.5	39	46	1.18
141	254.7	1.359	1.81	45	8.8	52	60	1.15
142	254.3	1.322	1.65	40	7.4	72	79	1.10
143	253.8	1.285	1.51	35	6.2	93	100	1.08
144	253.4	1.255	1.24	25	4.2	110	125	1.14
145	104.1	1.567	1.94	49	10.1	12	15	1.25
146	104.4	1.537	2.06	53	11.4	12	14	1.17
147	104.7	1.507	1.88	47	9.6	13	16	1.23
148	105.1	1.463	2.17	56	12.8	14	19	1.36
149	105.4	1.433	2.09	54	11.8	18	22	1.22
150	105.8	1.403	2.23	58	13.4	21	25	1.19
151	106.3	1.359	2.33	61	14.7	25	29	1.16
152	106.6	1.329	2.40	63	15.5	29	34	1.17
153	107.0	1.300	1.76	43	8.3	34	40	1.18
154	107.4	1.270	1.48	34	5.9	43	50	1.16
155	107.8	1.241	1.65	40	7.4	49	55	1.12
156	108.2	1.211	1.67	41	7.5	57	62	1.09
157	108.7	1.182	1.73	42	8.1	72	78	1.08
158	109.2	1.153	1.75	43	8.2	76	82	1.08
159	109.9	1.109	1.21	24	3.9	91	108	1.19
			Slit II (2)					
160	248.1	1.697	1.94	49	10.1	5	8	1.60
161	247.7	1.669	1.32	28	4.7	6	9	1.50
162	247.3	1.640	2.09	54	11.8	6	9	1.50
163	246.9	1.612	1.72	42	8.0	6	10	1.67
164	246.4	1.584	1.35	29	4.9	8	12	1.50
165	246.0	1.556	1.17	22	3.7	9	15	1.67

Table 3 - continued

1.	2.	3.	4.	5.	6.	7.	8.	9.
166	245.5	1.528	1.32	28	4.7	10	19	1.90
167	245.0	1.500	1.65	40	7.3	11	24	2.18
168	244.5	1.472	1.90	48	9.8	13	31	2.38
169	242.8	1.363	1.91	48	9.9	28	77	2.75
170	241.6	1.336	1.44	33	5.6	46	92	2.00
171	240.9	1.309	1.50	35	6.1	58	103	1.78
172	240.3	1.282	1.34	29	4.8	75	126	1.68
173	238.8	1.230	1.13	21	3.5	104	333	3.20
174	115.5	1.528	0.68	0	1.3	9	15	1.67
175	116.0	1.500	1.20	24	3.9	11	19	1.73
176	116.5	1.472	1.55	36	6.5	11	18	1.64
177	117.0	1.445	1.52	35	6.2	12	21	1.75
178	117.6	1.417	1.68	41	7.6	14	28	2.00
179	118.2	1.390	1.88	47	9.6	16	33	2.06
180	118.8	1.363	1.70	41	7.8	23	43	1.87
181	119.4	1.336	1.57	37	6.6	27	47	1.74
182	120.1	1.309	1.71	42	7.9	31	54	1.74
183	120.8	1.282	1.51	35	6.1	42	63	1.50
184	121.5	1.256	1.52	35	6.2	51	71	1.39
185	122.2	1.230	1.17	22	3.7	64	79	1.23
186	123.0	1.203	1.27	26	4.4	77	84	1.09
187	123.8	1.178	1.43	32	5.5	85	96	1.13
188	124.6	1.152	0.69	0	1.3	99	114	1.15
189	125.5	1.127	1.10	19	3.3	104	127	1.22
190	126.4	1.102	1.38	31	5.1	132	256	1.94
			Slit I (1)					
191	218.5	1.425	2.05	53	11.3	40	46	1.15
192	217.5	1.406	2.03	52	11.1	42	48	1.14
193	216.5	1.388	1.91	48	9.9	48	55	1.15
194	215.4	1.370	2.06	53	11.4	49	55	1.12
195	214.4	1.353	1.21	24	3.9	53	58	1.09
196	213.3	1.336	1.64	40	7.3	53	58	1.09
197	212.2	1.319	2.04	52	11.2	57	61	1.07
198	209.2	1.281	1.18	23	3.8	66	68	1.03
199	146.1	1.361	1.54	36	6.4	17	21	1.24
200	148.8	1.319	2.21	58	13.2	20	25	1.25

Table 3 - continued

1.	2.	3.	4.	5.	6.	7.	8.	9.
201	151.8	1.280	2.14	55	12.5	26	30	1.15
202	154.9	1.245	2.10	54	11.8	32	41	1.28
203	158.2	1.214	2.32	61	14.5	47	54	1.15
204	161.6	1.187	1.71	42	7.9	62	68	1.10
205	168.9	1.147	1.52	35	6.3	93	100	1.08
			Slit I (2)					
206	213.9	1.677	1.35	29	4.9	12	17	1.42
207	213.0	1.660	0.72	0	1.4	12	18	1.50
208	212.1	1.644	1.23	25	4.1	12	17	1.42
209	211.2	1.628	1.61	39	7.0	12	16	1.33
210	209.8	1.605	1.44	33	5.6	13	19	1.46
211	208.3	1.583	1.42	32	5.4	15	22	1.47
212	206.3	1.555	1.45	33	5.7	16	25	1.56
213	204.8	1.535	1.28	27	4.4	19	26	1.37
214	203.2	1.517	1.56	37	6.5	21	28	1.33
215	201.0	1.495	1.31	28	4.6	24	28	1.17
216	199.3	1.479	1.10	19	3.2	26	32	1.23
217	197.6	1.465	1.32	28	4.7	29	36	1.24
218	195.3	1.448	1.74	43	8.2	30	38	1.27
219	193.5	1.437	1.25	26	4.2	34	38	1.12
220	191.7	1.427	1.54	36	6.4	34	40	1.18
221	189.3	1.416	1.72	42	8.0	35	41	1.17
222	187.4	1.410	1.20	24	3.9	38	41	1.08
223	185.5	1.405	1.03	16	2.9	42	45	1.07
224	183.0	1.401	1.10	19	3.3	43	54	1.26
225	181.0	1.400	1.28	27	4.4	42	50	1.19
226	156.3	1.536	1.13	21	3.5	9	10	1.11
227	158.9	1.506	1.33	29	4.8	10	13	1.30
228	161.1	1.484	1.72	42	8.0	12	16	1.33
229	162.8	1.469	1.23	25	4.1	15	20	1.33
230	164.6	1.456	1.68	41	7.6	18	23	1.28
231	166.9	1.440	1.36	30	5.0	24	32	1.33
232	168.7	1.430	1.45	33	5.7	28	36	1.29
233	170.5	1.421	1.93	49	10.0	31	38	1.23
234	172.4	1.414	1.23	25	4.1	31	40	1.29
235	174.2	1.408	1.52	35	6.2	31	39	1.26
236	179.2	1.400	0.96	12	2.5	38	42	1.11

Table 4

Line-of-sight velocities derived from the red coronal line

No.	Position angle	$R/R_\odot$	v kms^{-1}
1.	2.	3.	4.
	Slit IV(1)		
1	320.1	1.495	1
2	321.0	1.475	1
3	321.9	1.456	1
4	322.9	1.437	0
5	323.9	1.418	- 5
6	324.9	1.400	- 6
7	325.9	1.383	- 1
8	327.0	1.365	- 2
9	328.1	1.348	0
10	329.2	1.332	1
11	330.3	1.317	- 7
12	331.5	1.301	- 3
13	332.7	1.287	3
14	333.9	1.273	- 1
15	335.2	1.259	0
16	336.5	1.247	- 1
17	337.8	1.234	2
18	339.1	1.223	1
19	340.5	1.219	- 1
20	341.8	1.202	- 1
21	343.2	1.192	0
22	344.7	1.183	1
23	346.1	1.175	- 2
24	349.1	1.162	4
25	350.5	1.156	8
26	352.0	1.151	5
27	353.6	1.147	5
28	355.1	1.144	11
29	356.6	1.141	7
30	358.2	1.139	4

Table 4 - continued

1.	2.	3.	4.
31	359.7	1.139	3
32	1.3	1.139	2
33	2.8	1.141	3
34	4.4	1.143	4
35	5.9	1.147	0
36	7.4	1.151	8
37	9.0	1.156	2
38	10.0	1.162	- 1
39	12.0	1.168	2
40	13.4	1.175	5
41	14.9	1.183	3
42	16.3	1.192	5
43	17.8	1.202	3
44	19.2	1.212	- 1
45	20.5	1.223	1
46	21.9	1.234	1
47	23.2	1.247	- 2
48	24.5	1.259	- 2
49	25.8	1.273	- 2
50	27.1	1.287	- 7
51	28.3	1.302	- 2
52	29.5	1.317	- 3
53	30.7	1.332	- 1
54	31.8	1.349	- 4
55	32.9	1.365	- 8
56	34.0	1.383	1
57	35.1	1.400	- 6
58	36.1	1.418	- 4
59	37.1	1.437	- 1
60	38.1	1.456	- 1
61	40.0	1.475	- 8
62	40.9	1.495	- 5
63	41.8	1.515	- 3
64	42.7	1.536	- 8
65	43.5	1.557	- 3

Table 4 - continued

1.	2.	3.	4.
66	44.3	1.578	- 6
67	45.1	1.599	-10
68	45.9	1.621	- 3
69	46.6	1.643	- 8
70	47.3	1.665	- 9
	Slit IV (2)		
71	312.1	1.297	0
72	313.1	1.274	- 1
73	314.0	1.251	1
74	315.0	1.229	2
75	316.0	1.207	3
76	317.1	1.186	5
77	318.2	1.165	5
78	319.3	1.145	10
79	320.5	1.125	10
80	53.8	1.440	- 7
81	53.0	1.415	- 2
82	52.2	1.391	- 2
83	51.4	1.367	- 1
84	50.6	1.343	0
85	49.8	1.320	- 4
86	48.9	1.297	- 3
87	48.0	1.274	- 1
88	47.0	1.251	- 4
89	46.0	1.229	- 3
90	45.0	1.208	- 3
91	43.9	1.186	- 5
92	42.8	1.165	0
93	41.7	1.145	- 1
	Slit III (1)		
94	284.2	1.631	1
95	284.4	1.600	- 4
96	284.7	1.571	-10
97	285.0	1.541	- 2
98	285.3	1.511	0
99	285.6	1.482	- 3
100	285.9	1.452	- 4

Table 4 - continued

1.	2.	3.	4.
101	286.2	1.422	- 4
102	286.5	1.392	1
103	286.9	1.363	0
104	287.3	1.333	- 1
105	287.7	1.304	5
106	288.1	1.275	4
107	288.5	1.245	9
108	289.0	1.216	- 1
109	289.4	1.187	11
110	289.9	1.158	10
111	290.4	1.129	14
112	77.3	1.690	3
113	77.1	1.660	- 4
114	76.9	1.631	- 7
115	76.6	1.601	- 5
116	76.3	1.571	- 9
117	76.0	1.541	- 6
118	75.8	1.511	- 7
119	75.5	1.482	- 4
120	75.1	1.452	- 3
121	74.8	1.422	- 6
122	74.5	1.393	- 4
123	74.1	1.363	- 2
124	73.7	1.334	- 5
125	73.3	1.304	- 4
126	72.9	1.275	- 7
127	72.5	1.245	- 3
128	72.1	1.216	- 6
129	71.6	1.187	0
130	71.1	1.158	1
	Slit III (2)		
131	274.6	1.496	- 1
132	274.7	1.465	- 3
133	274.8	1.435	- 2
134	274.9	1.404	0
135	275.0	1.373	- 1

Table 4 - continued

1.	2.	3.	4.
136	275.1	1.343	1
137	275.2	1.312	4
138	275.3	1.281	6
139	275.4	1.251	5
140	275.6	1.220	5
141	275.7	1.189	4
142	86.7	1.619	0
143	86.6	1.588	- 2
144	86.5	1.557	- 2
145	86.5	1.527	- 5
146	86.4	1.496	- 3
147	86.3	1.465	- 5
148	86.2	1.435	- 8
149	86.1	1.404	- 8
150	86.0	1.373	- 8
151	85.9	1.342	- 4
152	85.8	1.312	- 3
153	85.7	1.281	- 2
154	85.6	1.251	- 2
155	85.4	1.220	- 4
156	85.3	1.189	- 3
157	85.2	1.159	- 4
158	85.0	1.128	- 4
	Slit II (1)		
159	256.3	1.507	11
160	256.0	1.477	6
161	255.7	1.448	9
162	255.4	1.418	1
163	255.1	1.388	3
164	254.7	1.359	0
165	254.4	1.329	1
166	254.0	1.300	5
167	253.6	1.270	1
168	253.2	1.241	- 9
169	252.8	1.211	- 3
170	252.3	1.182	- 4

Table 4 - continued

1.	2.	3.	4.
171	104.1	1.567	7
172	104.4	1.537	1
173	104.7	1.507	5
174	105.0	1.478	- 4
175	105.3	1.448	1
176	105.6	1.418	14
177	106.0	1.388	- 7
178	106.3	1.359	- 2
179	106.6	1.329	- 8
180	107.0	1.300	- 3
181	107.4	1.270	- 2
182	107.8	1.241	-17
183	108.2	1.211	-11
184	108.7	1.182	- 6
185	109.2	1.153	- 3
186	109.7	1.124	-10
187	110.2	1.095	- 8
	Slit II (2)		
188	247.1	1.626	- 3
189	246.6	1.598	- 5
190	246.2	1.570	- 4
191	245.7	1.542	0
192	245.2	1.514	0
193	244.7	1.486	4
194	244.2	1.459	7
195	242.5	1.376	8
196	241.9	1.349	3
197	241.3	1.322	4
198	240.6	1.296	1
199	239.9	1.269	4
200	239.2	1.242	5
201	238.4	1.216	0
202	237.6	1.190	5
203	117.3	1.431	1
204	117.9	1.404	3
205	118.5	1.376	2

Table 4 - continued

1.	2.	3.	4.
206	119.1	1.349	- 1
207	119.7	1.322	1
208	120.4	1.296	0
209	121.1	1.269	1
210	121.8	1.243	- 4
211	122.6	1.217	- 1
212	123.4	1.190	- 8
213	124.2	1.165	- 8
214	125.0	1.139	- 8
215	126.0	1.114	- 4
216	126.9	1.089	1
	Slit I (1)		
217	218.5	1.425	7
218	217.5	1.406	8
219	216.5	1.387	12
220	215.5	1.370	8
221	214.4	1.353	6
222	213.3	1.335	4
223	212.2	1.319	- 3
224	211.0	1.303	- 6
225	207.4	1.259	- 1
226	204.8	1.232	- 1
227	202.2	1.208	12
228	198.0	1.177	1
229	195.1	1.160	- 2
230	190.6	1.140	1
231	182.9	1.124	4
232	175.0	1.128	- 1
233	167.4	1.153	- 7
234	165.9	1.160	-13
235	164.5	1.168	- 1
236	163.0	1.177	- 3
237	161.6	1.187	- 8
238	160.2	1.197	- 8
239	158.8	1.208	- 1
240	157.5	1.220	4

Table 4 - continued

1.	2.	3.	4.
241	156.2	1.232	6
242	154.9	1.245	8
243	153.6	1.259	11
244	152.4	1.273	14
245	151.2	1.288	7
246	150.0	1.303	7
247	148.8	1.319	13
248	147.7	1.335	10
249	146.6	1.353	5
250	145.6	1.370	3
251	144.5	1.387	14
252	143.5	1.406	5
253	142.5	1.425	- 1
	Slit I (2)		
254	208.8	1.590	3
255	207.8	1.576	1
256	206.8	1.562	8
257	205.8	1.548	3
258	204.8	1.536	3
259	203.7	1.523	6
260	202.6	1.511	3
261	201.5	1.500	4
262	200.4	1.489	6
263	199.3	1.479	4
264	198.2	1.469	6
265	197.0	1.460	10
266	195.9	1.452	11
267	194.7	1.444	8
268	193.5	1.437	5
269	192.3	1.430	- 1
270	191.1	1.424	9
271	189.9	1.419	4
272	188.6	1.414	- 7
273	187.4	1.410	- 5
274	186.1	1.407	- 3
275	184.9	1.404	- 3

Table 4 - continued

1.	2.	3.	4.
276	183.6	1.402	1
277	182.4	1.401	0
278	181.1	1.400	2
279	179.9	1.400	2
280	178.6	1.401	5
281	174.9	1.407	7
282	173.6	1.410	6
283	172.4	1.414	4
284	171.1	1.419	3
285	169.9	1.424	5
286	168.7	1.430	2
287	167.5	1.437	- 4
288	166.3	1.444	- 1
289	165.1	1.452	2
290	164.0	1.460	- 3
291	162.8	1.469	- 2
292	161.7	1.479	- 1
293	160.6	1.489	- 2
294	159.5	1.500	- 1
295	158.4	1.511	- 6
296	157.3	1.523	- 5
297	156.3	1.535	- 9
298	155.2	1.548	- 5
299	154.2	1.562	- 5
300	153.2	1.576	- 5

CHAPTER 3

THE 1983 CORONA: 5303 Å LINE PROFILES

3.1. Introduction

At the 1980 eclipse the coronal spectra were obtained in the line 6374 Å (Chapter 2). Similar information collected from the simultaneous observations using two of the emission lines during an eclipse would extend our concept manyfold of the distribution of temperature within the corona. With this aim we used the multislit technique to obtain coronal spectra simultaneously in the two lines 6374 Å [Fe X] and 5303 Å [Fe XIV] with a good coverage over the solar corona at the eclipse of June 11, 1983.

The characteristics of the red coronal line have been given in Chapter 2 and those of the green line are (Allen 1973)

Transition	=	$3p,\ ^2P_{1/2} - {}^2P_{3/2}$
Transition probability	=	$60\ s^{-1}$
Excitation potential	=	2.34 eV
Ionization potential	=	355 eV
Average equivalent width of the eclipse coronal line in terms of electron scatter (K) continuum	=	20 Å

Temperature at which Fe XIV ion is most abundant (Jordan 1969) = 2.3×10^6 K

The experiment was set up at a site (Long. 112° 21' 28" E; Lat. 6° 51' 54"; elevation a few metres), very close to the central path of totality, near Paciran in East Java. The general features of the eclipse at this site were

	Local time	P	V	Solar Altitude	Solar Azimuth
First contact	$9^h\ 59^m\ 35^s$	249°	29°	-	-
Second contact	$11^h\ 33^m\ 52^s$	67°	247°	59°	2°
Third contact	$11^h\ 38^m\ 59^s$	257°	81°	60°	358°
Fourth contact	$13^h\ 16^m\ 31^s$	76°	300°	-	-

Duration of totality = $5^m\ 07^s$

Magnitude of the eclipse = 1.037

Width of the eclipse path = 200 km

Local time = U.T. $+7^h\ 00^m$

P = angle of contact on the solar disc measured from the north point through east.

V = angle measured from the vertex of the solar image.

The sky was covered with thin bands of cirrus clouds during the phase of totality.

The experiment was planned to give twice the spatial resolution as compared to that of 1980. Unfortunately the spectra in 6374 Å are underexposed and hence not very useful. We present here the results of the analysis of the 5303 Å line spectra.

3.2. Instruments

A two-mirror 30 cm coelostat, with Zerodur optics, was used to feed the sun light to the telescope objective. The main wheel of the first coelostat mirror was driven by friction through a metallic tape which in turn was driven by a well regulated stepper motor. The coelostat was adjusted to direct the light so that the rotation axis of the sun was always in the direction of the length of the slits. A schematic sketch of the experimental set up is shown in Figure 19. An objective of 15 cm aperture and 225 cm focal length formed a 20.7 mm image of the sun on the plane of the five slits of the spectrograph. These slits separated by 5 mm corresponding to 7.8 arcmin on the solar image had widths of 60 micron each providing a spatial resolution of 5.5 arcsec. A pelicle beam splitter (T = 92%, R = 8%) mounted in front of the slits allowed a

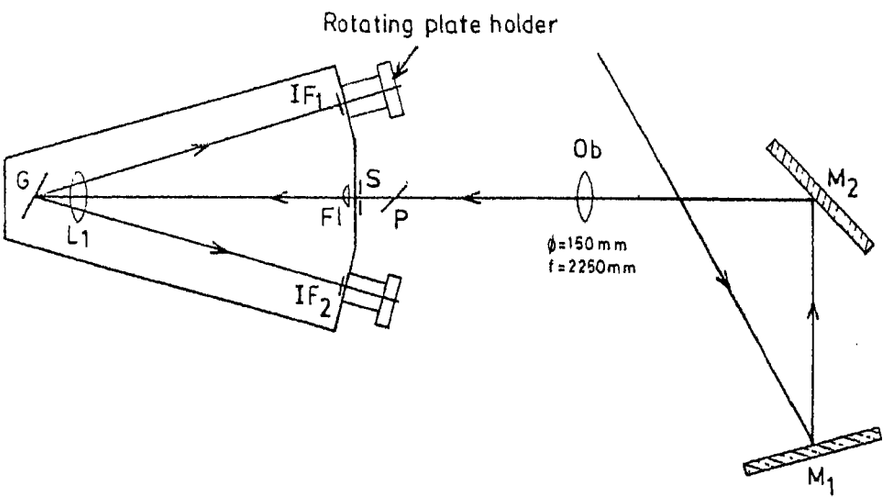

Fig. 19: A schematic sketch of the experimental set up for observing 6374 Å and 5303 Å lines simultaneously. M_1 and M_2 = flat mirrors; Ob = objective; P = pelicle beam splitter (T = 92%, R = 8%); S = multislit; Fl = field lens. L_1 = collimator (ϕ = 150 mm, f = 2250 mm); G = grating (600 lines mm^{-1}) and IF_1 and IF_2 = interference filters.

simultaneous recording of coronal and comparison spectra. The field lens F_1 placed just behind the slits focussed the objective lens onto the collimating lens and thus avoided the over-spilling of the beam. A grating with 600 lines mm^{-1} blazed at 2.0 micron in the first order along with a 225 cm focal length doublet achromat lens in the Littrow mode gave a dispersion of 2.17 mm^{-1} in the third order.

The spectrograph was designed to record the spectra in 5303 Å and 6374 Å lines simultaneously using a single stage Varo image intensifier on each wavelength. The image intensifier had a gain of 20 and an effective aperture of 30 mm. The interference filters of 10 Å band width having peak transmission at 6376 Å and 5305 Å were placed in front of the respective image tubes to cut off the undesired continuum. A turret plate-holder which could hold six photographic plates at a time and permitted quick change of plates after each exposure was used. The plates were exposed by keeping the emulsion in contact with the fibre optic face plate of the image intensifier. The spectrum of [Fe X] has a neon comparison line at 6382.99 Å for the measurement of the line-of-sight velocities and instrumental line profile.

3.3. Observations

Four spectra in each wavelength were obtained during the totality. Two of these spectra in the 5303 Å line exposed for 30 s and 50 s respectively were found to be properly exposed. Figure 20 shows a reproduction of the 50 s exposure spectra. The spectra exposed on Kodak 103-aD emulsion were developed in D-19 at a temperature of 20 C for five minutes together with the step wedge calibration obtained through the same image tube and the Kodaikanal 18 m spectrograph. Neon spectra of 6382.99 Å line obtained along the entire length of the five slits permitted the evaluation of the instrumental line profiles at several points on each slit. The full width at half maximum (FWHM) of these instrumental line profiles at several points on each slit is roughly the same and its mean value 0.35 ± 0.04 Å was used for the determination of coronal line widths. Spectra from four slits appeared well on the photographic plate; that of the fifth slit at 1.13 $R_\odot$ near the north pole is not registered well because of insufficient intensity. Microphotometer scans of these spectra were made using a projected slit of 5.5 x 9 arcsec^2, successive scans being separated by 9 arcsec along the slit. These scans were then converted into intensities by following the regular photometric procedure.

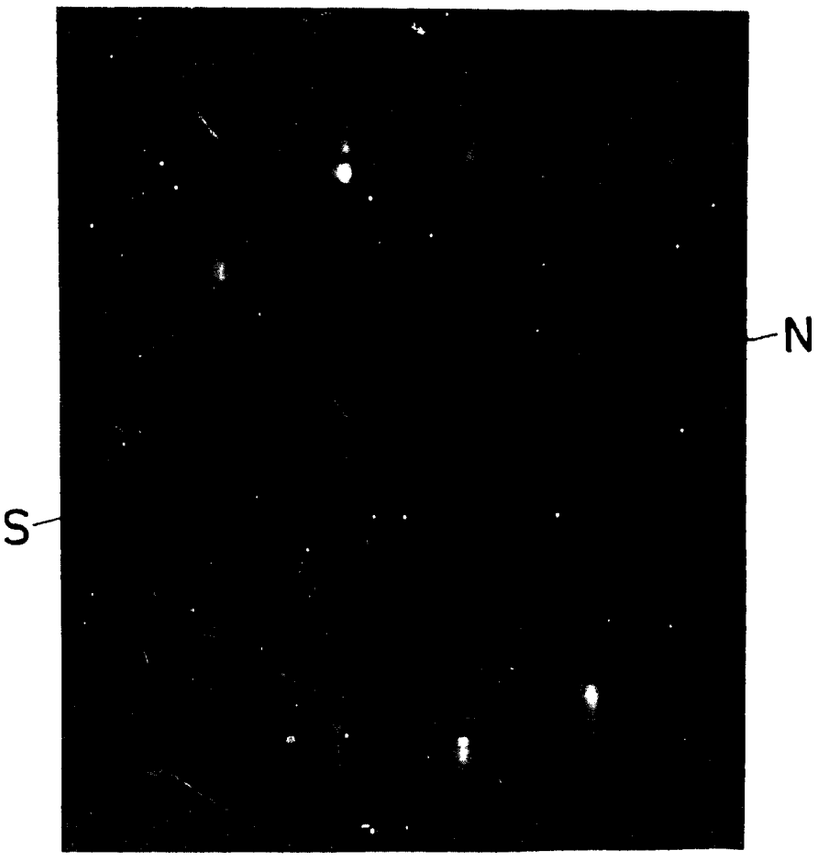

Fig.20: Spectra of 5303 Å line of eclipse of June 11, 1983 with multislit. Exposure = 50 s. N-S represents the rotation axis of the sun.

3.4. Results

From these line profiles the line widths of the green coronal line were measured at 113 locations within the solar corona ranging from 1.04 to 1.24 $R_\odot$. The data are presented in Table 5. The position angle measured from the north point of the projected axis of the solar rotation and the radial distance from the centre of the disc are given in columns 2 and 3. Column 4 gives the FWHM values and column 5 the turbulent velocities derived by assuming a coronal temperature of 2.3×10^6 K. Column 6 contains the equivalent temperature if the FWHM is ascribed entirely to thermal broadening. The relative intensities of the line are listed in column 7 and the relative line-of-sight velocities in column 8.

Line widths

One of the typical observed line profiles (open circles) and the best Gaussian fit to these data points (full line) are presented in Figure 21. The FWHM measured from free hand curves and the Gaussian curves agree with each other well and the difference if any does not exceed 3 per cent. The measured line widths were corrected for the instrumental width as was done for the 1980 eclipse data. Figure 22 shows the FWHM

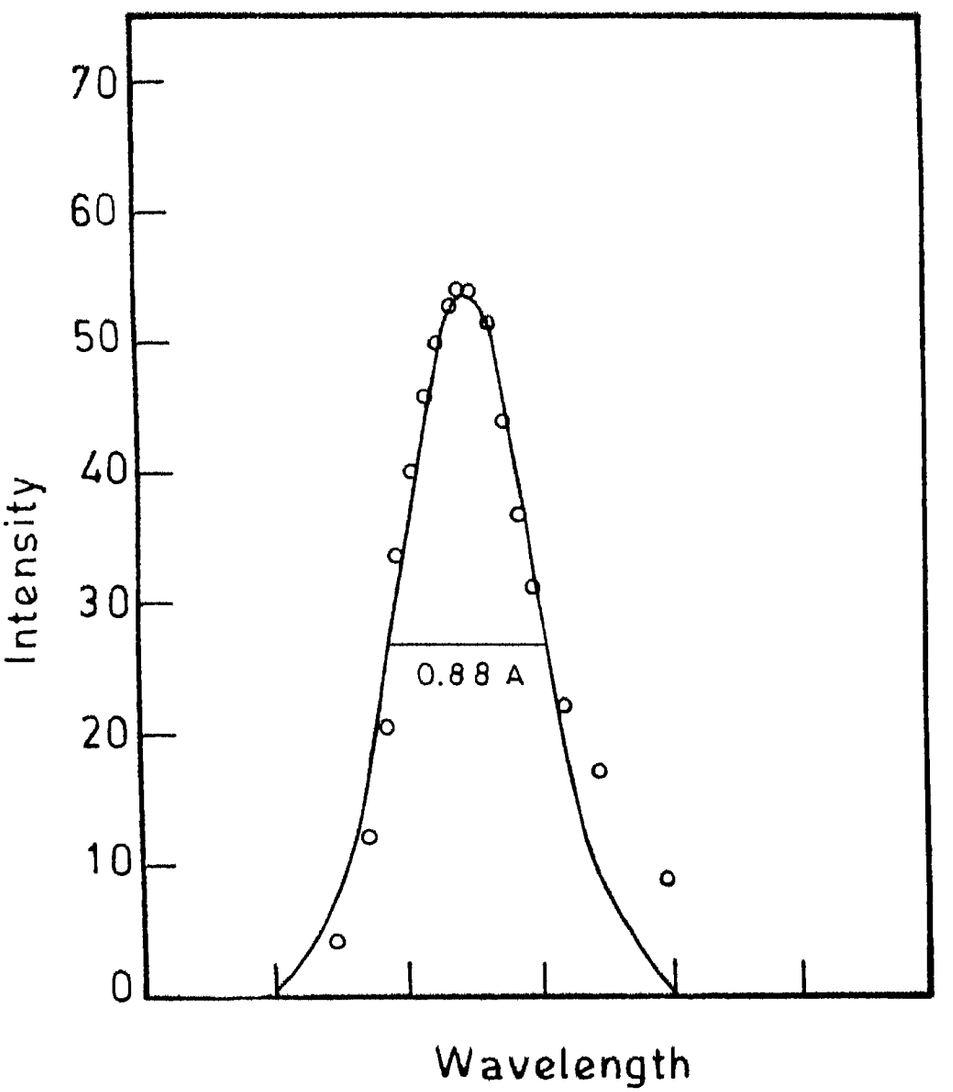

Fig. 21: A typical observed line profile of 5303 Å line. Full line curve is the best Gaussian fit to these data points.

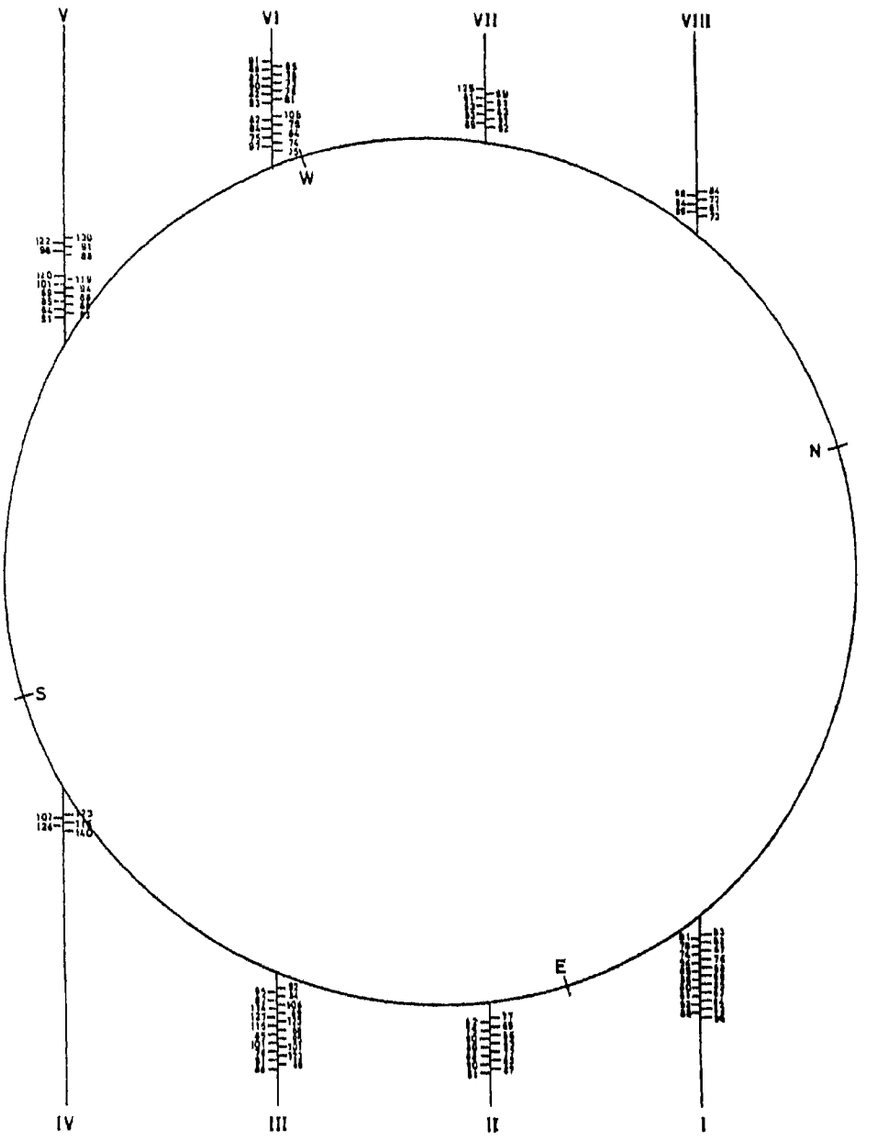

Fig. 22: The numbers represent the true line widths of the 5303 Å line in units of Å x 10^{-2} at various locations. Position of the slits have been marked as I, II, III etc. for identification.

at various locations in the solar corona. The frequency distribution of the line widths is presented in Figure 23. The line widths vary from 0.6 Å to 1.4 Å and, if wholly due to thermal broadening, correspond to a temperature range of $1.4 - 6.5 \times 10^6$ K. The most frequent line width of 0.9 Å implies a kinetic temperature of 3.1×10^6 K. Line widths against the radial distance in six different direction are shown in Figure 24. The plot of the mean line width against radial distance is shown in Figure 25. The individual plots shown in Figure 24 indicate the presence of line width maximum around 1.1 $R_\odot$, but in the average curve of Figure 25 the existence of the maximum becomes marginal.

Line intensities

Relative intensities of the various peaks of line profiles are used for the study of gradients of the emission corona. A logarithmic representation of these intensities against the radial distance is shown in Figure 26 at four slit positions. The emission gradients are steep for very small values of $R/R_\odot$ except at a position angle of $\theta = 125°$.

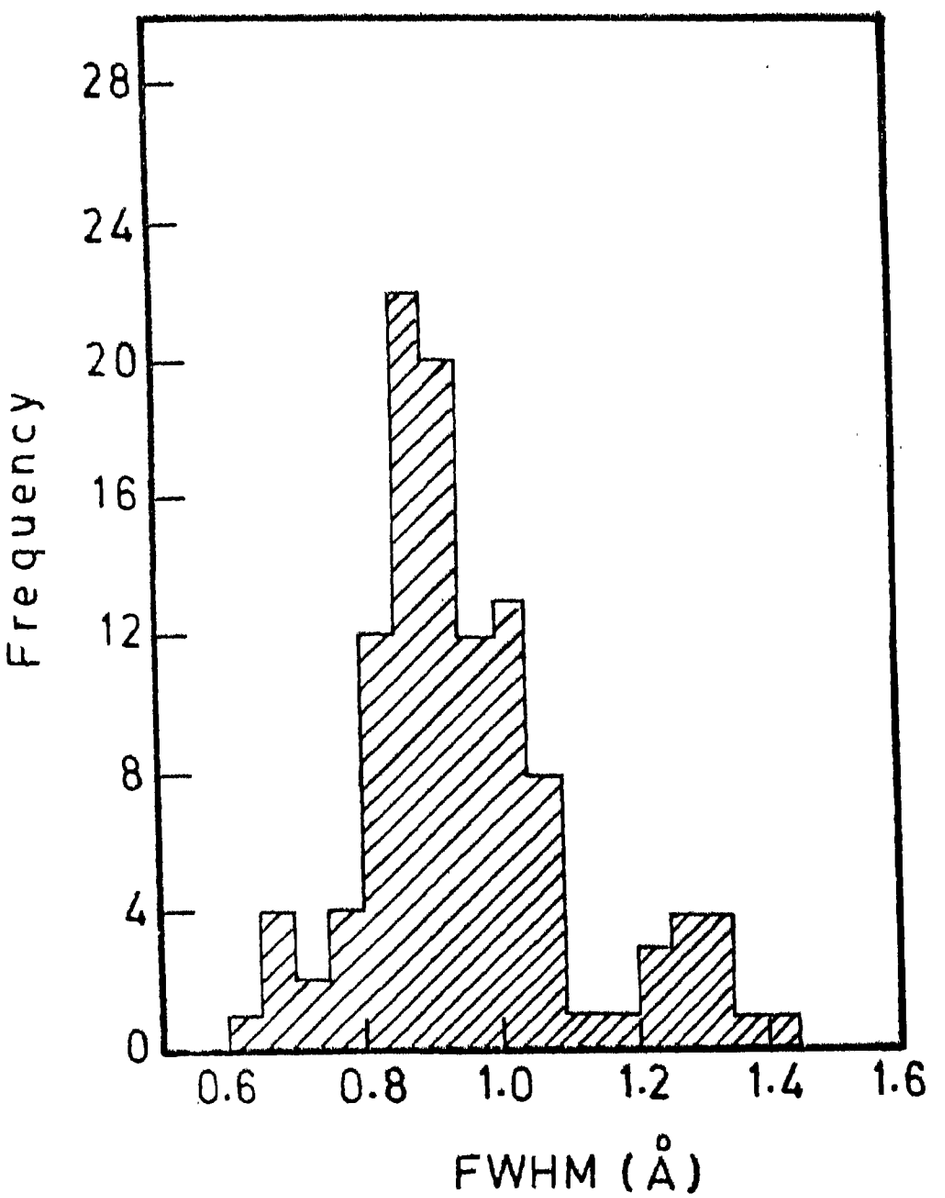

Fig. 23: The frequency distribution of the line width of 5303 Å.

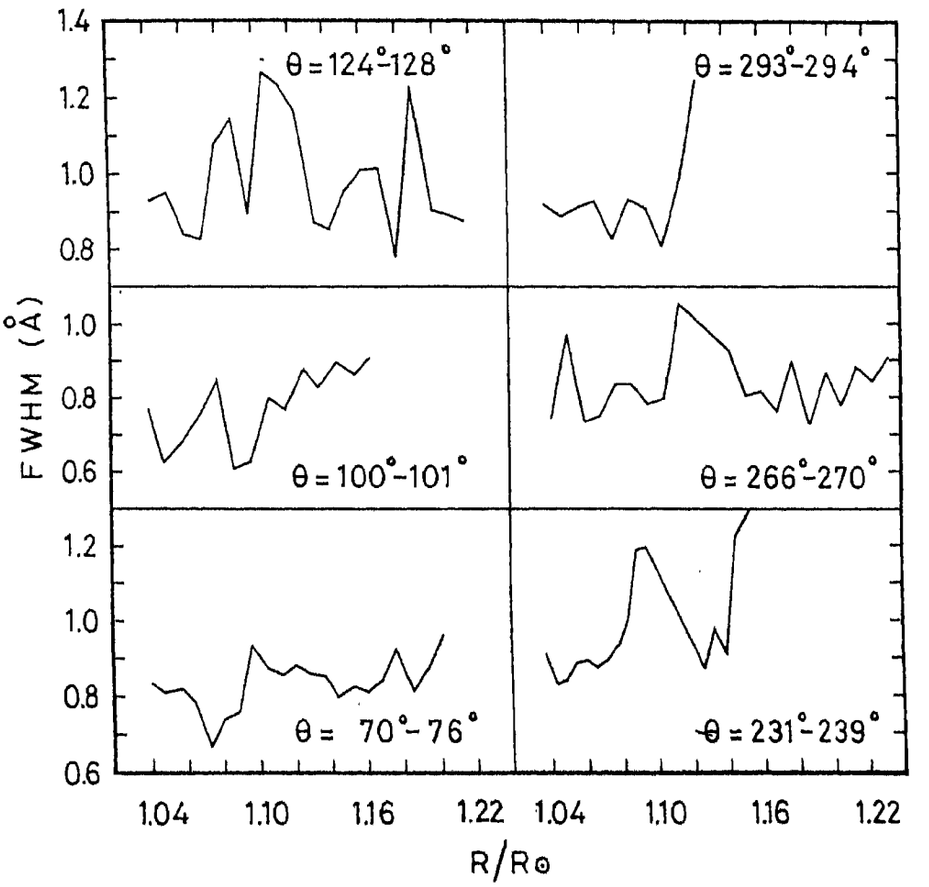

Fig. 24: Variations of the line widths with radial distance in different directions. Position angle is also indicated for each curve.

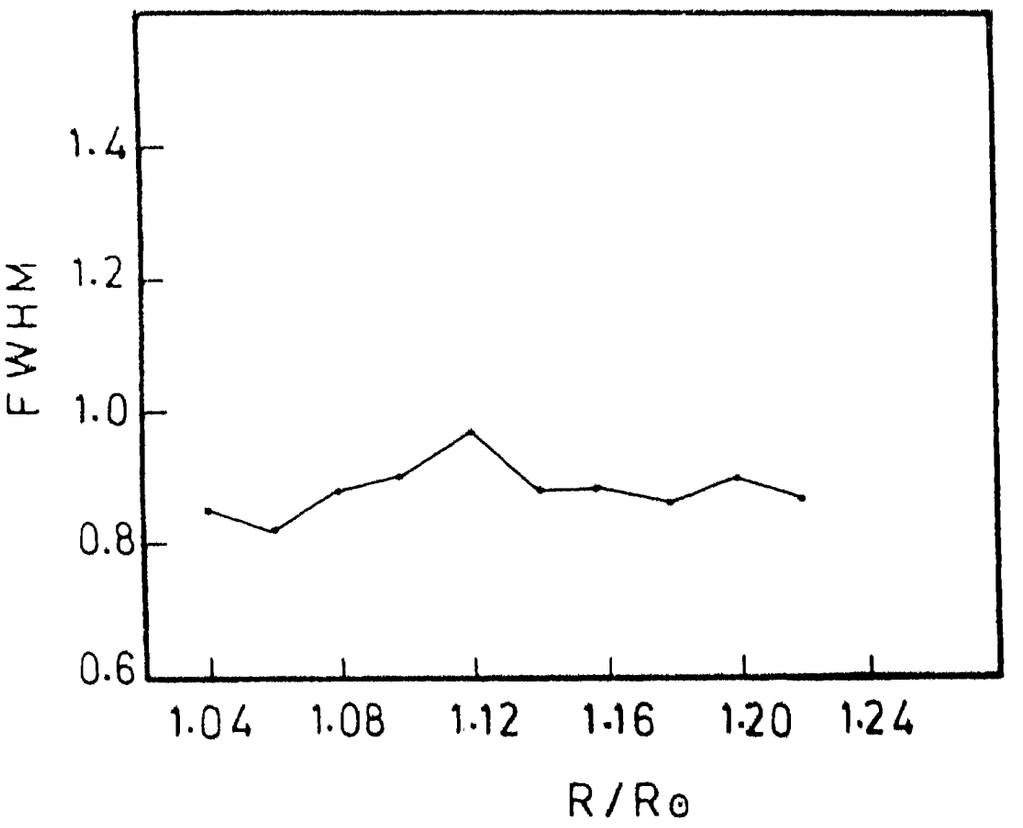

Fig.25: Average variation of the line width with radial distance.

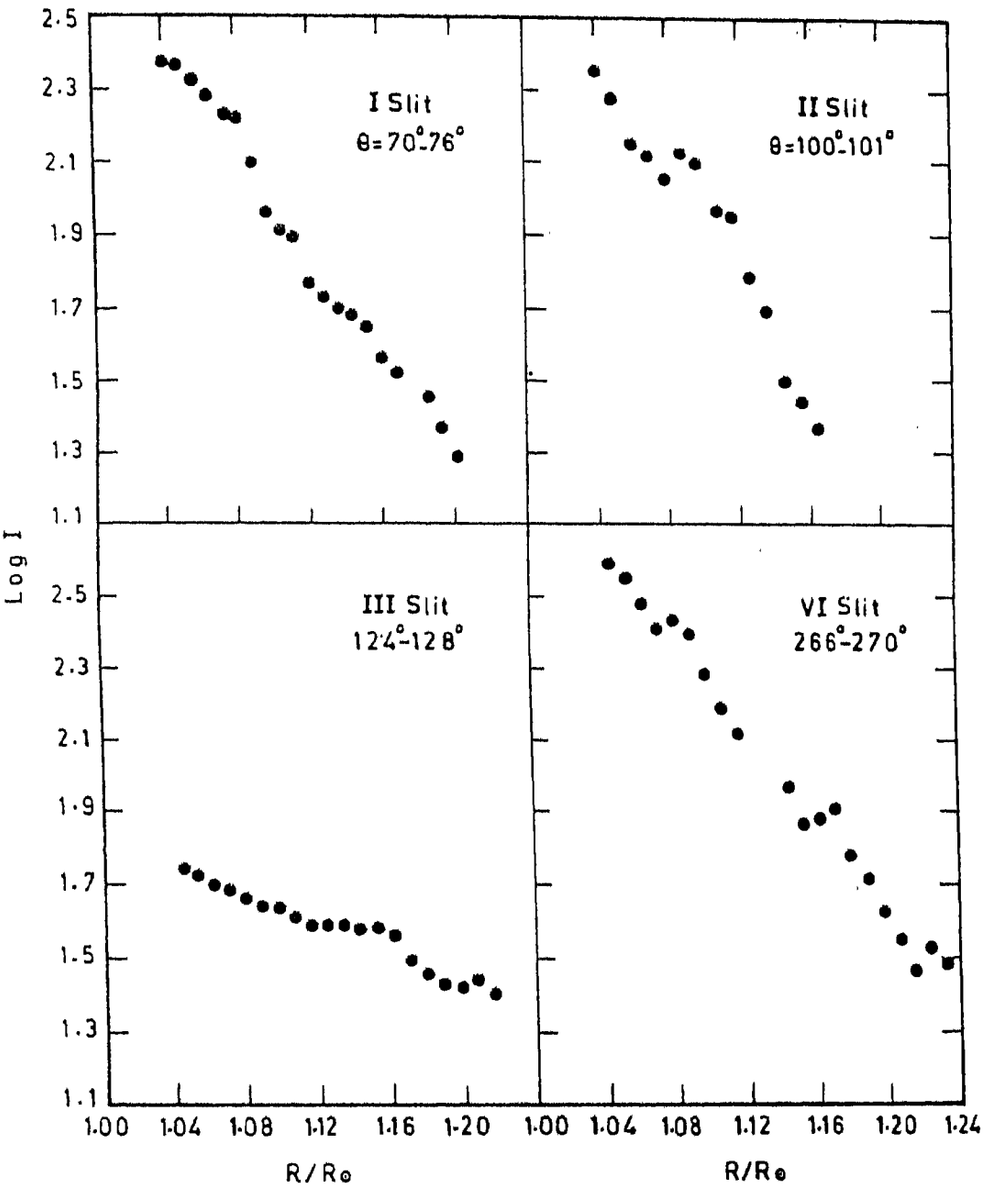

Fig.26: Intensity of 5303 Å line in logarithmic units against radial distance. Position angle is indicated for each curve.

Line-of-sight velocities

In the absence of a comparison line for the 5303 Å spectra, Doppler shifts were measured with reference to a fiducial mark etched on the plate. Assuming a zero residual velocity along the whole length of the slit, we have derived the relative line-of-sight velocities for the two central slits for which there is practically no distortion of the spectra due to the pin-cushion effect in the image tube.

The line-of-sight velocities on most of the locations turn out to be within $\pm$ 5 kms^{-1}, indicating that the corona is remarkably quiet (Livingston and Harvey 1982; Singh, Bappu and Saxena 1982). Had there been large scale mass motions in the solar corona, as reported by Delone and Makarova (1969) and Desai, Chandrasekhar and Angreji (1982), the measured line-of-sight velocities would have been much larger than the observed values of $\pm$ 5 kms^{-1}.

Table 5

Line widths, intensities and turbulent velocities derived from the green coronal line

No.	Position angle θ	$R/R_\odot$	FWHM Å	V_t Kms^{-1}	Temp.	I_1	v Kms^{-1}
1.	2.	3.	4.	5.	6.	7.	8.
			I Slit				
1	70.53	1.040	0.832	10.7	2.7	235	-
2	70.85	1.048	0.811	8.5	2.5	231	-
3	71.16	1.056	0.819	9.4	2.6	212	-
4	71.46	1.064	0.776	3.0	2.3	190	-
5	71.76	1.072	0.667	0.0	1.7	166	-
6	72.06	1.080	0.737	0.0	2.1	162	-
7	72.35	1.088	0.763	0.0	2.3	123	-
8	72.64	1.096	0.936	18.0	3.4	97	-
9	72.92	1.104	0.876	14.1	2.9	81	-
10	73.20	1.112	0.854	12.5	2.8	77	-
11	73.47	1.120	0.884	14.7	3.0	58	-
12	73.75	1.128	0.858	12.8	2.9	53	-
13	74.01	1.136	0.854	12.5	2.8	50	-
14	74.28	1.144	0.798	7.0	2.5	47	-
15	74.54	1.152	0.823	9.8	2.6	44	-
16	74.80	1.160	0.810	8.5	2.5	37	-
17	75.04	1.168	0.841	11.4	2.7	32	-
18	75.29	1.176	0.923	17.2	3.3	28	-
19	75.54	1.185	0.815	9.0	2.6	28	-
20	75.78	1.193	0.876	14.1	3.0	23	-
21	76.02	1.201	0.962	19.6	3.6	19	-
			II Slit				
22	100.06	1.040	0.771	1.2	2.3	224	0.7
23	100.12	1.049	0.624	0	1.5	187	-1.2
24	100.19	1.059	0.685	0	1.8	142	0
25	100.25	1.068	0.754	0	2.2	133	-2.5
26	100.31	1.078	0.858	12.8	2.9	112	-2.0
27	100.37	1.087	0.602	0	1.4	133	0
28	100.43	1.097	0.628	0	1.5	124	1.7
29	100.48	1.107	0.802	7.5	2.5	92	0
30	100.54	1.116	0.767	0	2.3	89	-3.2

Table 5 - continued

1.	2.	3.	4.	5.	6.	7.	8.
31	100.59	1.126	0.884	14.7	3.0	60	+2.5
32	100.65	1.135	0.832	10.7	2.7	49	-1.2
33	100.70	1.145	0.897	15.6	3.1	31	3.7
34	100.75	1.155	0.867	13.5	2.9	28	0.5
35	100.81	1.164	0.910	16.4	3.2	23	2.5
			III Slit				
36	127.62	1.043	0.928	17.5	3.3	56	1.2
37	127.43	1.052	0.949	18.8	3.5	53	-2.0
38	127.25	1.061	0.841	11.4	2.7	50	0
39	127.07	1.070	0.824	9.9	2.6	49	1.0
40	126.89	1.079	1.079	25.7	4.5	46	2.7
41	126.72	1.088	1.144	28.7	5.0	44	5.6
42	126.55	1.097	0.893	15.3	3.1	44	10.0
43	126.38	1.106	1.270	34.3	6.2	41	-7.8
44	126.22	1.115	1.232	32.6	5.9	39	5.6
45	126.06	1.124	1.153	29.1	5.2	39	-2.9
46	125.90	1.134	0.876	14.1	3.0	39	-0.5
47	125.74	1.142	0.850	12.1	2.8	38	-3.7
48	125.59	1.152	0.954	19.1	3.5	39	-0.5
49	125.43	1.161	1.006	21.9	3.9	36	-3.0
50	125.29	1.170	1.010	22.2	4.0	31	0
51	125.14	1.179	0.780	4.1	2.4	29	1.0
52	125.00	1.188	1.232	32.6	5.9	27	-4.6
53	124.85	1.198	0.906	16.2	3.2	26	-0.5
54	124.71	1.207	0.893	15.3	3.1	28	-0.5
55	124.57	1.216	0.876	14.1	2.9	25	-3.4
			IV Slit				
56	162.40	1.045	1.232	32.6	5.9	27	-
57	161.96	1.050	1.071	25.2	4.4	27	-
58	161.54	1.056	1.149	28.9	5.1	22	-
59	161.11	1.061	1.258	33.7	6.1	19	-
60	159.86	1.079	1.397	39.5	7.5	15	-
			V Slit				
61	231.16	1.039	0.910	16.4	3.2	94	-
62	231.60	1.045	0.832	10.7	2.7	84	-
63	232.04	1.050	0.837	11.0	2.7	72	-
64	232.46	1.055	0.884	14.7	3.0	67	-
65	232.89	1.061	0.893	15.3	3.1	68	-

Table 5 - continued

1.	2.	3.	4.	5.	6.	7.	8.
66	233.31	1.067	0.876	14.1	3.0	75	-
67	233.73	1.073	0.893	15.3	3.1	74	-
68	234.14	1.079	0.936	18.0	3.4	65	-
69	234.54	1.085	1.006	21.9	3.9	44	-
70	234.95	1.090	1.188	30.7	5.5	43	-
71	235.34	1.096	1.197	31.1	5.5	41	-
72	237.27	1.127	0.876	14.1	3.0	26	-
73	237.64	1.133	0.984	20.8	3.8	26	-
74	238.01	1.140	0.910	16.4	3.2	27	-
75	238.37	1.146	1.223	32.2	5.8	21	-
76	238.74	1.152	1.296	35.4	6.5	19	-
			VI Slit				
77	266.38	1.043	0.746	0	2.1	394	2.5
78	266.57	1.052	0.971	20.0	3.6	354	-0.0
79	266.75	1.061	0.737	0	2.1	303	4.9
80	266.93	1.070	0.746	0	2.1	257	2.5
81	267.10	1.079	0.837	11.0	2.7	275	-2.5
82	267.28	1.088	0.837	11.0	2.7	251	-2.5
83	267.45	1.097	0.789	5.7	2.4	194	-4.6
84	267.62	1.106	0.802	7.5	2.5	155	2.0
85	267.78	1.115	1.062	24.8	4.4	133	0.7
86	268.26	1.143	0.932	17.8	3.4	94	0
87	268.41	1.152	0.806	8.0	2.5	74	1.7
88	268.56	1.161	0.819	9.4	2.6	77	-2.5
89	268.71	1.170	0.763	0	2.3	83	-1.5
90	268.86	1.179	0.902	15.9	3.1	61	-1.0
91	269.00	1.189	0.728	0	2.1	53	-2.0
92	269.15	1.198	0.867	13.5	2.9	43	-1.2
93	269.29	1.207	0.780	4.1	2.4	36	0
94	269.43	1.216	0.884	14.7	3.0	30	0
95	269.57	1.225	0.850	12.1	2.8	34	1.2
96	269.70	1.234	0.910	16.4	3.2	31	-4.4
			VII Slit				
97	293.94	1.040	0.919	17.0	3.3	76	-0.5

Table 5 - continued

1.	2.	3.	4.	5.	6.	7.	8.
98	293.88	1.049	0.889	15.0	3.1	61	-0.5
99	293.81	1.059	0.910	16.4	3.2	61	-2.5
100	293.75	1.068	0.927	17.5	3.3	52	-1.0
101	293.69	1.078	0.832	10.7	2.7	44	-3.2
102	293.63	1.087	0.932	17.8	3.4	39	1.0
103	293.57	1.097	0.906	16.1	3.2	33	-2.0
104	293.52	1.106	0.811	8.5	2.5	28	6.4
105	293.46	1.116	0.989	21.0	3.8	27	3.9
106	293.40	1.126	1.249	33.3	6.0	21	-3.4
			VIII Slit				
107	323.47	1.040	0.732	0	2.1	54	-
108	323.15	1.048	0.893	15.3	3.1	38	-
109	322.84	1.056	0.606	0	1.4	36	-
110	322.54	1.064	0.641	0	1.6	36	-
111	322.24	1.072	0.715	0	1.9	26	-
112	321.94	1.080	0.876	14.1	2.9	19	-
113	321.65	1.088	0.836	11.0	2.7	15	-

CHAPTER 4

THE 1983 CORONA: CORONAL ROTATION

4.1. Introduction

The experiments described in Chapters 2 and 3 were meant for the study of the spatial properties of the coronal line profiles in the 6374 Å and 5303 Å lines. They do not contain sufficient information about the regions near the poles. Therefore, an experiment was set up at the 1983 eclipse to determine the flow pattern near the poles and to measure the coronal rotation. Spectra near the poles were too small in extent to permit a study of the flow pattern at the poles, and the spectra near the east and the west limb were not intense enough to permit an evaluation of the temperature structure. We could determine only the velocity structure and the coronal rotation from the 6374 Å emission line which are presented here.

4.2. Instruments

A 30 cm coelostat similar to the one used in 1980 was employed to direct the light to a 10 cm aperture objective of 100 cm focal length. The objective was an achromat Zeiss doublet and formed

a 9.2 mm image of the sun in the slit plane of the spectrograph with three slits each 80 micron wide and separated by 5 mm from its neighbour. The slits were thus spaced at 17.2 arcmin on the solar image. The multislit spectrograph functioned in the Littrow mode, and was oriented such that the central slit was close to the poles of the imaged sun. A 600 lines mm^{-1} grating and a 100 cm focal length doublet achromat lens together provided a dispersion of 2.68 mm^{-1} in the fourth order red region. A broad band red filter was placed in front of the slits to cut off other orders of the spectrum. A 35 mm camera body carrying Kodak 103-aE film was used to photograph the spectra in the focal plane of the Littrow system. Neon comparison spectra were also recorded simultaneously to provide the wavelength calibration.

4.3. Observations

Two spectra of 100 s and 200 s exposure of the red line were obtained during the totality phase of the eclipse. The exposed Kodak 103-aE film was developed in D-19 at a temperature of 20 C for five minutes together with the photometric calibration. The 200 s spectra were found to be suitable for velocity measurements. The 6382.99 Å line of neon, being closer to the [Fe X] line than the 6402.25 Å

line, was used as the reference point. Microphotometer scans of these spectra were obtained with a spatial resolution of 17 x 17 arcsec^2 on the plate. The successive scans were separated by 17 arcsec along the slit. The separation between the peaks of 6382.99 Å neon line and the red line was used to derive the wavelength of the [Fe X] line.

4.4. Results

The wavelength of the red coronal line was derived at 57 locations ranging from 1.09 to 1.17 $R_\odot$. The data are presented in Table 6. The position angle measured from the north point of the projected axis of the sun and the radial distance from the centre of the disc are given in columns (2) and (3) respectively. The values of the wavelength of the red line are listed in column (4). Column (5) gives the line-of-sight velocities derived by using the mean wavelength 6374.604 Å for the red line. Out of the 57 locations at which the wavelength of the red coronal line was measured, 28 were on the east limb corona and 25 on the west limb, and the remaining four locations were near the south pole but none near the north pole. All values of the wavelength were corrected for the rotational velocity of the sun and

then used to derive the mean wavelength of the red line. The mean value turns out to be 6374.604 ± 0.03 Å, in good agreement with the value 6374.596 ± 0.02 Å derived at the 1980 eclipse (Chapter 2). The distribution of the line-of-sight velocities is shown in Figure 27. These velocities vary between +10 kms^{-1} and -14 kms^{-1} but most of the locations have velocities less than ± 5 kms^{-1}. The mean wavelength of the red line on the east limb corona is 6374.530 ± 0.04 Å and that on the west limb corona is 6374.678 ± 0.04 Å. The difference of 0.148 Å between these two values corresponds to a coronal rotation rate of 3.5 kms^{-1} and compares well with the photospheric value. The limited accuracy of our measures (probable error ± 1 kms^{-1}) and the presence of the small scale random velocities do not permit an estimation of differential rotation of the solar corona. We thus conclude from these data that the corona does not show any localized differential mass motion and corotates with the photospheric layers.

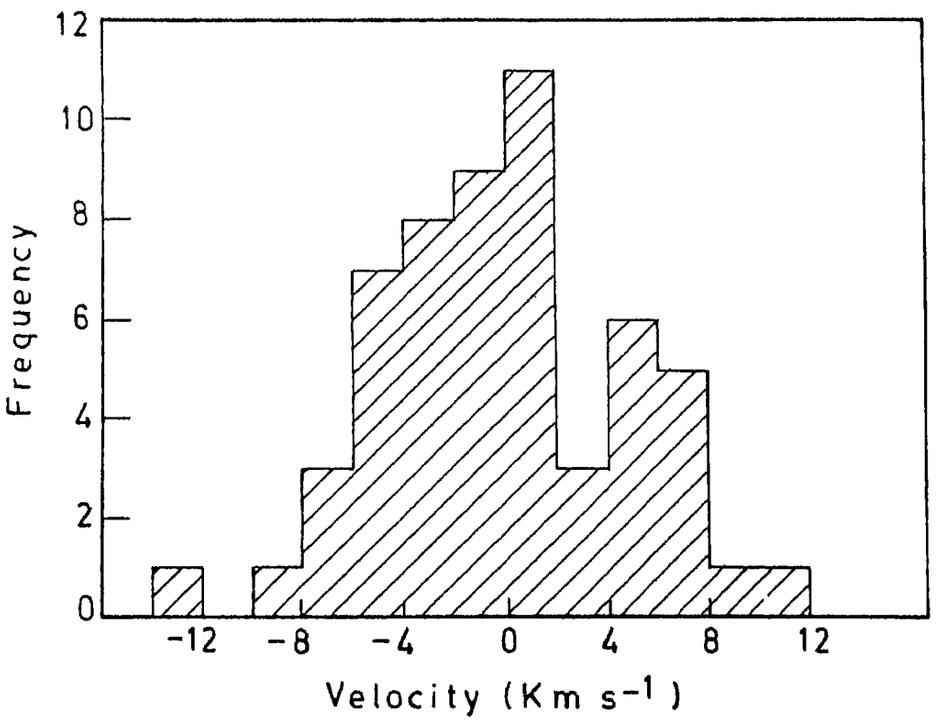

Fig. 27: Frequency distribution of the line-of-sight velocities as derived for 6374 Å.

Table 6

Wavelength of red coronal line and derived line-of-sight velocities

S.No.	Position angle	$R/R_\odot$	Wavelength	kms^{-1}
1.	2.	3.	4.	5.
		East (III slit)		
1	85.73	1.183	6374.544	- 2.8
2	86.71	1.175	6374.469	- 6.4
3	87.69	1.167	6374.308	-13.9
4	88.70	1.159	6374.442	- 7.9
5	89.71	1.152	6374.523	- 3.8
6	90.74	1.145	6374.512	- 4.3
7	91.78	1.138	6374.485	- 5.6
8	92.83	1.132	6374.523	- 3.8
9	93.89	1.126	6374.555	- 2.3
10	94.96	1.120	6374.512	- 4.3
11	96.05	1.115	6374.394	- 9.9
12	97.14	1.110	6374.496	- 5.1
13	98.24	1.106	6374.641	+ 1.7
14	99.35	1.103	6374.576	- 1.3
15	100.47	1.099	6374.533	- 3.3
16	101.59	1.096	6374.544	- 2.8
17	102.72	1.094	6374.523	- 3.8
18	103.86	1.092	6374.490	- 5.3
19	105.00	1.090	6374.448	- 7.4
20	106.14	1.088	6374.603	0.0
21	107.28	1.087	6374.576	- 1.3
22	108.43	1.087	6374.619	+ 0.7
23	109.57	1.087	6374.630	+ 1.2
24	110.71	1.087	6374.619	+ 0.7
25	111.86	1.088	6374.598	- 0.3
26	113.00	1.090	6374.630	+ 1.2
27	114.14	1.092	6374.565	- 1.8
28	115.29	1.094	6374.496	- 5.1

Table 6 - continued

1.	2.	3.	4.	5.
		II Slit Southpole		
29	199.00	1.033	6374.576	- 1.3
30	199.00	1.054	6374.523	- 3.8
31	199.00	1.076	6374.528	- 3.6
32	199.00	1.098	6374.624	+ 1.0
		West I Slit		
33	268.70	1.159	6374.748	+ 6.8
34	269.71	1.152	6374.737	+ 6.3
35	270.74	1.145	6374.710	+ 5.0
36	271.78	1.138	6374.598	- 0.3
37	272.83	1.132	6374.737	+ 6.3
38	273.89	1.126	6374.748	+ 6.8
39	274.96	1.120	6374.689	+ 4.0
40	276.05	1.115	6374.699	+ 4.5
41	277.14	1.111	6374.630	+ 1.2
42	278.24	1.106	6374.716	+ 5.3
43	279.35	1.103	6374.817	+10.0
44	280.47	1.099	6374.704	+ 4.8
45	281.59	1.096	6374.737	+ 6.3
46	282.72	1.093	6374.780	+ 8.3
47	283.86	1.091	6374.694	+ 4.2
48	284.99	1.090	6374.662	+ 2.7
49	286.14	1.088	6374.592	- 0.6
50	287.28	1.087	6374.630	+ 1.2
51	288.43	1.087	6374.619	+ 0.7
52	289.57	1.087	6374.672	+ 3.2
53	290.72	1.087	6374.694	+ 4.2
54	291.86	1.088	6374.619	+ 0.7
55	293.00	1.090	6374.496	- 5.1
56	294.14	1.091	6374.592	- 0.6
57	295.28	1.093	6374.640	+ 1.7

CHAPTER 5

DISCUSSION OF THE RESULTS

5.1. Comparison of line and continuum intensities

The contribution of the background K-corona to the visible portion of the electromagnetic spectrum is mainly due to the scattering of photospheric radiation into the line of sight. The mechanism of scattering is usually assumed to be Thompson scattering by free electrons. Thus the amount of scattered radiation in the optical continuum depends directly on the electron density. Line radiation arising from forbidden transitions depends solely on the number of ions in the excited level. This in turn depends on the mode of excitation to the level. If excitation is mainly collisional then this number is proportional to the square of the electron density and if radiative excitation is dominant, this number would simply be proportional to the electron density. As a consequence, the behaviour of the ratios I_l/I_c and I_l/I_c^2 (I_l = line intensity, I_c = continuum intensity) as a function of distance would give a clue to understand the dominant mode of excitation. The behaviour of these ratios has been described in Chapter 2. Here we shall summarise and discuss some

of the results on this point.

Billings (1966) had remarked on the difficulty of obtaining clear distinctions on the mode of excitation over extensive regions. It is not common to observationally distinguish these effects purely because of the difficulty in obtaining well exposed continuum over extensive regions. The data of 1980 eclipse provide a wide range, viz. $1.1 < R/R_\odot < 1.7$, for examination, since the continuum was indeed well exposed out to large distances in the corona.

The main points to be noted are that we do see three regions where the behaviour of I_1/I_c and I_1/I_c^2 is distinct. For $R/R_\odot < 1.2$ we see that I_1/I_c^2 is almost constant indicating collisional excitation. For $1.2 < R/R_\odot < 1.4$ I_1/I_c^2 is seen to increase with $R/R_\odot$ and I_1/I_c remains practically constant implying the dominance of radiative excitation over collisional excitation. After $1.4\ R_\odot$ the ratio I_1/I_c^2 increases with radial distance at a faster rate compared to that for $R/R_\odot < 1.4$. Thus collisional excitation seems to be less important in this region as compared to that for $R/R_\odot < 1.4$. This inturn indicates that radiative excitation becomes more important at larger $R/R_\odot$ values. Therefore, one can say that for $R/R_\odot < 1.2$ mode of excitation is more or less collisional; collisional

as well as radiative excitation is equally important for $1.2 < R/R_\odot < 1.4$; and for $R/R_\odot > 1.4$, radiative excitation becomes more dominant. At the same time one should note that these indicate only an average behaviour and are not meant to demarcate the boundary of the excitation modes. The coronal regions $R/R_\odot > 1.2$ in all directions show an increase of I_1/I_c^2 with radial distance and only 50 per cent of the directions indicate that I_1/I_c remains more or less unchanged. The other half of the directions show that I_1/I_c increases between $1.2 < R/R_\odot < 1.4$ and has a maximum value around 1.4 $R_\odot$. One way of interpreting the maximum value of I_1/I_c is to accept that it represents a maximum in the degree of ionization at 1.4 $R_\odot$ along these directions.

However, without an independent knowledge of the variation of electron density with distance, it is difficult to make any statement regarding the degree of ionization and hence the variation of temperature. It is, however, interesting to note that the region close to the south pole exhibits somewhat lower values of I_1/I_c and that this region happens to contain a coronal hole. The other information available from line profile is its width. The broadening of the line will consist of contributions from thermal as well as nonthermal motions. These parameters may vary

independently. Therefore, the line widths are of not much help in determining the temperature gradients.

5.2. Line widths

As described in Chapter 2, the derived values of FWHM of the red coronal line vary between 0.6 Å and 2.4 Å. A histogram of the line width dependence (Figure 8) shows a predominance of values of FWHM around 1.3 Å and an extended tail towards larger values. The lowest value of line width is 0.6 Å. If thermal broadening is the only contribution to line widths, then with the aid of the standard kinetic temperature formula one arrives at temperature of 1.2×10^6 K for a line width of 0.67 Å. Thus the peak value of 1.3 Å in the histogram, corresponds to a higher temperature of 4.6×10^6 K while the highest line width of 2.4 Å corresponds to an even higher temperature. However, electron density model predicts a temperature of about 1.4×10^6 K (van de Hulst 1953). The temperature from radio astronomical observations in the wavelength range 1-5 m has a value of about 1.1×10^6 K during the solar minimum and 1.8×10^6 K for quiet corona at the sunspot maximum (Leblanc and LeSqueren 1969). Assuming the solar corona to be in ionization equilibrium, Jordan (1969) has calculated the ionization

equilibrium as a function of temperature for several of the coronal ions. The computations indicate that Fe X ion is mostly available in the temperature zone $5 \times 10^5 - 2 \times 10^6$ K, with a peak at 1.3×10^6 K and Fe XIV ion has a maximum concentration at a temperature of 2.3×10^6 K. Under the assumption that Fe XIV is the most abundant ion, which is consistent with the mean intensity of 5303 Å line relative to other coronal lines, one would place the most common ionization temperature of the corona at about 2×10^6 K. At the same time, it must be recognized that the ionization temperature near 1.3×10^6 K (Fe X) are also relatively common in the normal corona. It, therefore, becomes inadmissible to accept the high values of temperature inferred from line widths, especially for a relatively low temperature ion like Fe X. This difficulty is partly overcome by assuming an additional line broadening agency which seems inescapable. Introducing a turbulence parameter in the equation, and assuming the ions of iron to be controlled by the peak value of 1.3×10^6 K (Jordan 1969), one arrives at turbulent velocity of the order of 30 kms^{-1} for the peak line width of 1.3 Å. Feldman and Behring (1974) showed, from the line profiles of highly ionized O, Mg, Si, S and Fe in the wavelength range 170 Å to 370 Å, the presence of a mean random turbulent velocity of

about 30 kms^{-1} in addition to thermal Doppler broadening. Mariska, Feldman and Doschek (1978) found that at a height of 8 arcsec all the lines (1000 Å - 3000 Å) formed at temperature above 4×10^4 K have an average nonthermal random velocity of about 28 kms^{-1} and it increases with height. From NRL Skylab data of 1445.76 Å [Si VIII], 1467.08 Å [Fe XI] and 1242.03 Å [Fe XII], Cheng, Doschek and Feldman (1979) derive a nonthermal velocity of 10-25 kms^{-1} at 1.7×10^6 K [Fe XII], 10-17 kms^{-1} at 1.5×10^6 K [Fe XI] and 10-20 kms^{-1} at 9.3×10^5 K [Si VIII]. This indicates that nonthermal velocities 10-30 kms^{-1} are common in the solar corona. The smallest values in the histogram of line width seem to be representative of the state of ionization. The larger FWHM must necessarily signify the appreciable contribution to it by Doppler motions. An evaluation of this characteristic is extremely difficult. For, in the line-of-sight of an optically thin gas, one witnesses besides the effect of thermal broadening, integration along the line of sight.

Detailed evaluation of the variation of this turbulence with location in the corona is clearly impossible with data with only one line. The non-homogeneous nature of the corona is evident from both

white light photographs and monochromatic pictures taken in green and red lines (Dollfus 1971; Dunn 1971). The contribution to line width from various other locations in the line of sight can broaden the line and account for excess width, if there are large macroscopic motions in the solar corona. But our value for the line-of-sight velocity of $\pm$ 5 kms^{-1} at most of the locations exclude the presence of macroscopic motions. Hence, the presence of turbulence is clear but a sensible assessment of either the variation of temperature or turbulence is not possible. However, certain broad characteristics can be inferred from our data. One striking feature is the difference between the line width seen in contiguous "open" field and "closed" field regions near the south pole. The mean value of line widths in the open field region, which contained a coronal hole, is 1.36 $\pm$ 0.26 Å (slit I(2)), whereas the mean of the line widths in a closed field region which contained helmets, in the mean direction of 157°, is 1.76 $\pm$ 0.38 Å (slit I(1)) and for another closed region at 215° (mean) it is 1.93 $\pm$ 0.33 Å (slit II(1)). The value of 1.36 Å for coronal hole coincides with the peak of the histogram. The mean value of the line width over the entire corona, excluding the coronal hole, is 1.48 $\pm$ 0.35 Å which is slightly higher than the mean value for the

coronal hole. Our measures of the line widths for coronal hole and general corona correspond to line width temperatures of 5.0×10^6 K and 6.0×10^6 K respectively. There is thus a temperature difference of about 1.0×10^6 K between coronal hole and the general corona. According to Munro and Withbroe (1972) the temperature in a coronal hole is lower than in the general corona by about 0.6×10^6 K. Thus we may attribute the difference of 0.4×10^6 K. to the excess of turbulence in the general corona over that in the coronal hole. It would be worth while to measure such line widths in coronal holes and to relate them with quiet corona free of coronal holes. This would lead to a better understanding of the nature of turbulence within coronal holes. The abnormally high value of the line width in the closed regions unaccompanied by any abnormalities in the ratio I_1/I_c also gives an important bearing on the nonthermal processes that could occur in those complex magnetic configurations seen at the neutral points of helmet and streamer structures.

Yet another characteristic that deserves comment is the general coincidence of the maxima in I_1/I_c and line width at 1.4 $R_\odot$. If this could be interpreted as a coincidence of maximum temperature and turbulence,

then it brings out the usefulness of line profile data for the observational study of the coronal heating mechanisms, which have hitherto received only mainly theoretical attention (e.g. Ionson 1983). A further point for entertaining such hopes comes from our data on 5303 Å [Fe XIV] obtained at the 1983 eclipse. The most frequent value of the line width is 0.9 Å. Once again using similar arguments of maximum availability of Fe XIV ion at 2.3×10^6 K (Jordan 1969) as done earlier for Fe X, one can infer a mean turbulence of about 16 kms^{-1}. The fact that the corona was more active in 1980 than in 1983, coupled with the fact that the mean level of turbulence is correspondingly smaller in 1983, indicates the possibility of the variation of turbulence with activity. A further fact that may be considered is that the topology of magnetic fields is more 'closed' during solar maxima implying a hotter corona.

The above considerations clearly indicate the necessity of obtaining similar data during future eclipses. An independent estimation of temperature is, however, essential if more information is desired about the coronal heating mechanisms. The relevant experiments that have to be performed in this connection will be described in the next section.

5.3. Proposed experiments for future eclipses

(i) The high resolution multislit spectroscopy has provided considerable amount of information about the structure of the solar corona. During this study it was felt that the turbulence could have been better understood by observing the solar corona simultaneously in two lines originating from two ions of different atomic weights.

On an examination of the list of the coronal emission lines in the visible region one finds the two lines 4087 Å of [Ca XIII] and 6702 Å of [Ni XV] offer a good possibility when observed simultaneously. Both lines have different atomic weights but fall in class III which is characterized by an ionization potential between 400 eV and 650 eV (Jefferies, Orrall and Zirker 1971). Therefore, the emission in these lines will be occurring from more or less the same coronal regions. Hence, one can assume that by observing in these lines, one is looking at the same coronal regions having same temperatures. Therefore,

$$T = \frac{m_{Ca}}{2k} \frac{c^2 \Delta\lambda_{Ca}^2}{\lambda_{Ca}^2 \, 4 \ln 2}$$

$$T = \frac{m_{Ni}}{2k} \frac{c^2 \Delta\lambda_{Ni}^2}{\lambda_{Ni}^2 \, 4 \ln 2} .$$

By comparing the two line profiles, observed at the same location in the solar corona, one can directly compute the turbulence parameter. One should note that these lines are weak but if observations are secured only at a few locations they would provide information on turbulence.

(ii) To have more confidence in the derived value of the temperature, it is felt that simultaneous spectra should be taken in two strong emission lines whose ionization potential values are as close to each other as possible. The two emissions lines 6374 Å [Fe X] and 7892 Å [Fe XI] are potential candidates for this experiment. The ionization potentials for [Fe X] and [Fe XI] lines are 235 eV and 262 eV respectively. Therefore, emissions in these lines would mostly originate from the same temperature region of the corona. Spectrograms of high resolution using these lines would provide adequate data for this purpose. The broadening of these lines will yield a line width temperature whereas the ratio of these intensities will give the ionization temperature of the particular location. The excess line width temperature, if any, over the ionization temperature should be interpreted as due to random motions in the solar corona and hence as a direct observational evidence for the existence of turbulence in the solar corona.

(iii) The other important parameter is the electron density in the solar corona. It is customary to derive the electron density distribution from broad band photographs of the solar corona obtained with a polarigraph. This method, although most popular, contains inherent uncertainties and more so if attempted photographically. If one can photograph two emission lines originating from the fine structure levels of the ground term of an ion one can directly obtain the electron density from the intensity ratio of these lines. For instance the intensity ratios of the [Fe XIII] lines; I_{3388}/I_{10747} and I_{10747}/I_{10798} are almost independent of the temperature but dependent on the electron density. Theoretically we know the above ratios as a function of electron density (Dumont and Perche 1964). Therefore, by knowing the observed ratios one could infer the electron density in the emitting region from the theoretical curves. Of course, these lines fall in wavelength range beyond the range of the emulsions commonly in use. But with image tubes or charge coupled devices (CCD), one can plan to record the spectra of these three lines with good spatial resolution and derive the electron densities using the intensity ratios.

5.4. Summary of the conclusions

1. The behaviour of the line intensity and continuum intensity with radial distance indicates that for $R/R_\odot < 1.2$ mode of excitation is more or less collisional. Collisional as well as radiative excitation is equally important for $1.2 < R/R_\odot < 1.4$, and beyond $R/R_\odot = 1.4$ radiative excitation becomes more dominant.

2. From line width measurements, it is concluded that turbulent velocities of the order of 30 kms^{-1} were present in the corona at the time of the eclipse of 1980 and about 16 kms^{-1} during 1983. Therefore, it appears that the turbulence might be a function of solar activity, being higher when the sun is more active.

3. The spatial distribution of the line width measures showed that a maximum occurred around $1.4 \pm 0.1\ R_\odot$ during 1980 eclipse whereas similar results of the eclipse of 1983 do not indicate any such maximum.

4. The line-of-sight velocities measured range between +14 kms^{-1} to -17 kms^{-1} for the 1980 eclipse and those in 1983 lie between +12 kms^{-1} to -14 kms^{-1}. Most of the locations have velocities less than

$\pm$ 6 kms^{-1} during both the eclipses. From these observations one can conclude that there are no large scale localized differential mass motions in the corona.

5. The line-of-sight velocities also indicate that the corona corotates with the photospheric layers deeper down.

REFERENCES

Allen, C.W. 1973, Astrophysical Quantities, Athlone Press, p. 179.

Athay, R.G. 1975, The Solar Chromosphere and Corona: Quiet Sun, D. Reidel.

Billings, D.E. 1966, A Guide to the Solar Corona, Academic Press.

Burgess, A. 1964, Astrophys. J. 139, 776.

Burgess, A. and Seaton, M.J. 1964, Mon. Not. R. astr. Soc. 127, 355.

Cheng, C.C., Doschek, G.A. and Feldman, U. 1979, Astrophys. J. 227, 1037.

Cooper, R.H. and Billings, D.E. 1962, Z. Astrophys. 55, 24.

Cram, L.E. 1976, Solar Phys. 48, 3.

Delone, A.B. and Makarova, E.A. 1969, Solar Phys. 9, 116.

Delone, A.b. and Makarova, E.A. 1975, Solar Phys. 45, 157.

Desai, J.N., Chandrasekhar, T. and Angreji, P.D. 1982, J. Astrophys. Astr. 3, 69.

Desai, J.N., Chandrasekhar, T. 1983, J. Astrophys. Astr. 4, 65.

Dollfus, A. 1971, in Physics of Solar Corona (ed. C.J. Macris), D. Reidel, p. 97.

Dumont, J.P. and Perche, J.C. 1964, in Les Spectres Infrarouges des Astres, Inst. Astrophys. Cointe-Sclessin, Belgium, p. 186.

Dunn, R.B. 1971, in Physics of the Solar Corona (ed. C.J. Macris), D. Reidel, p. 114.

Edlen, B. 1942, Z. Astrophys. 22, 30.

Feldman, U. and Behring, W.E. 1974, Astrophys. J. Letters, 189, L45.

Goldberg, L., Dupree, A.K. and Allen, J.W. 1965, Ann. Astrophys. 28, 589.

Grotrian, W. 1931, Z. Astrophys. 3, 199.

Hirschberg, J.G., Wouters, A. and Hazelton, L. Jr. 1971, Solar Phys. 21, 448.

Ionson, J.A. 1983, IAU Symp. No.102, p. 391.

Jarrett, A.H. and von Klüber, H. 1955, Mon. Not. R. astr. Soc. 115, 343.

Jarrett, A.H. and von Klüber, H. 1961, Mon. Not. R. astr. Soc. 122, 223.

Jefferies, J.T., Orrall, F.Q. and Zirker, J.B. 1971, Solar Phys. 16, 103.

Jordan, C. 1969, Mon. Not. R. astr. Soc. 142, 501.

Kaliniak, A.A. 1949, Rep. Solar Eclipse Expt. of 1941, Sept. 21, Akademia Nauk U.S.S.R., Moscow, p. 352.

Keller, C.F. 1982, Proc. Indian natn. Sci. Acad. 48A, Suppl. No.3, p. 33.

Kim, I.S. and Nikolsky, G.M. 1975, Solar Phys. 43, 351.

Leblanc, Y. and LeSqueren, A.M. 1969, Astr. Astrophys. 1, 239.

Liebenberg, D.H., Bessey, R.J. and Watson, B. 1975, Solar Phys. 44, 345.

Livingston, W., Harvey, J. and Doe, L. 1970, Solar Eclipse 1970 Bulletin F, National Science Foundation, Washington, p. 72.

Livingston, W. and Harvey, J. 1982, Proc. Indian natn. Sci. Acad. 48A, Suppl. No.3, p. 18.

Lyot, B. 1939, Mon. Not. R. astr. Soc. 99, 580.

Lyot, B. 1950, Comp. Rend. Acad. Sci. Paris 231, 461.

Mariska, J.T., Feldman, U. and Doschek, G.A. 1978, Astrophys. J. 226, 698.

Mariska, J.T. and Withbroe, G.L. 1978, Solar Phys. 60, 67.

Marshall, P.M and Henderson, G. 1973, Solar Phys. 33, 153.

Menzel, D.H. and Pasachoff, J.M. 1968, Publ. astr. Soc. Pacific 80, 458.

Mitchell, S.A. 1935, Eclipses of the Sun, Columbia University Press.

Munro, R.H. and Withbroe, G.L. 1972, Astrophys. J. 176, 511.

Reeves, E.M., Vernazza, J.E. and Withbroe, G.L. 1976, Phil. Trans. R. Soc. Lond. A 281, 319.

Singh, J., Bappu, M.K.V., and Saxena, A.K. 1982, J. Astrophys. Astr. 3, 249.

Sivaraman, K.R. et al. 1984, J. Astrophys. Astr. 5, (in press).

Smartt, R.N., Zirker, J.B. and Mauter, H.A. 1982, Proc. Indian natn. Sci. Acad. 48A, Suppl. No.3, p. 102.

Trellis, M. 1957, Ann. Astrophys. Suppl. 5.

van de Hulst, H.C. 1953; in The Sun (ed. G.P. Kuiper), University of Chicago Press, p. 207.

Waldmeier, M. 1950, Z. Astrophys. 27, 24.

Withbroe, G.L. 1970, Solar Phys. 11, 42.

Withbroe, G.L. 1975, Solar Phys. 45, 301.

--